Pergamon

PII: S0301-9322(96)00054-7

Int. J. Multiphase Flow Vol. 23, No. 1, pp. 155–182, 1997

0301-9322/97 $17.00 + 0.00

PARTICLES IN A SHEAR FLOW NEAR A SOLID WALL: EFFECT OF NONSPHERICITY ON FORCES AND VELOCITIES

E. GAVZE[1] and M. SHAPIRO[2]

[1]Israel Institute for Biological Research, P.O. Box 19, Ness-Ziona 74100, Israel

[2]Faculty of Mechanical Engineering, Technion—Israel Institute of Technology, Haifa 32000, Israel

(Received 8 March 1995; in revised form 30 July 1996)

Abstract—Hydrodynamic forces and velocities of spheroidal particles in a simple shear flow near a solid wall are calculated by a variant of the boundary integral equation method, combined with the use of the reciprocal theorem for Stokes flow equations.

It is shown that the effect of the wall decreases with increasing particle nonsphericity (decreasing aspect ratio). For long slender particles the effective distance where the wall effect is significant is measured by several particle shorter axes. In the vicinity of the wall spheroids experience several interactions, which do not exist for spheres. These are the lift force component perpendicular to the wall and the corresponding rotational–translational coupling component of the resistance tensor.

The data on particle hydrodynamic interactions are used to calculate the velocities of the inertialess spheroidal particles in a shear flow near a wall. The calculations reveal that the effect of the wall is to create a nonzero velocity component in the direction of the normal to the wall surface. This velocity is zero for spheroids in a free shear flow; near the wall it vanishes for spherical and, seemingly, for oblong particles. Therefore a spheroid moving in a shear flow near the wall will perform an oscillatory motion towards and away from the wall. The wall will retard the particle motion parallel to its surface, albeit in a lesser extent than for spheres. In addition, spheroidal particles will perform periodic rotational motion, as they do in an unbounded shear flow, however, with larger periods. For force components which act on spheres, as well as on nonspherical particles the wall effect is most pronounced for particles whose shape is close to spherical.

Several correlation formulae are proposed for the forces and torques acting on spheroids, as well as for their friction tensor coefficients. Copyright © 1996 Elsevier Science Ltd.

Key Words: spheroidal particles, hydrodynamic resistance tensor, orientation, wall effect, lift and retardation velocities, rotational period

1. INTRODUCTION

Hydrodynamic interactions and transport of particles in flows are governed by their shapes. This factor significantly affects trajectories of particles moving in various flow fields under the influence of external forces. Small micrometer and submicrometer particles oftentimes possess shapes which significantly differ from spherical. Examples can be provided by fibrous aerosol particles generated in wool and cotton industries, asbestos particles, which received much attention in the literature because of their hazardous effect on human health. Other examples of nonspherical particles include red blood cells, large polymer molecules, fractal agglomerates, etc.

Motion of nonspherical particles in an infinite fluid has been extensively studied (see, e.g. Happel and Brenner 1983; Kim and Karrila 1991). Proximity of solid walls and/or free boundaries produce additional difficulties in obtaining analytical solutions for forces acting on nonspherical particles moving in viscous flows. However, in numerous industrial, technological and physiological applications particles often move close to solid walls. To name a few one can mention motion of aerosol particles in human and animals' respiratory tracks, in the vicinity of wafers during VLSI production, in sampling tubes (Ingham and Yan 1994), spectrometers and porous filters. Liquidborne particles experience wall interactions during their motion through various narrow constrictions, e.g. blood cells flowing in arteries; macromolecules moving in porous membranes, etc.

This work is devoted to investigation of hydrodynamic interactions between a nonspherical particle moving in a shear flow and a plane solid wall. The simple shear flow is met in lubrication

bearings; moreover, its importance is generally understood in connection with various flow situations, where the velocity distribution in the proximity to impermeable walls can be approximated as a linear function of the normal coordinate. These are flows in turbulent and laminar boundary layers, tubes, in the vicinity of sedimenting larger particles, etc. Generally, one can assume a simple shear to prevail near a solid wall in calculation of particle–wall viscous hydrodynamic interactions when the particle size a is significantly less than the dimension d of the vessel (e.g. tube diameter, channel width), or thickness d of the dynamic boundary layer (Shapiro and Goldenberg 1993; Bernstein and Shapiro 1994).

Theoretical analysis of particle motion in a quiescent fluid near a wall have been obtained for spherical particle shape in semi-infinite geometries (Brenner 1961; O'Neill 1964; Goldman *et al.* 1967a,b) and bounded geometries (Ganatos *et al.* 1980). Jeffrey and Onishi (1981) considered cylindrical particles near a plane wall. More complicated nonspherical particle geometries generally do not allow analytical solutions. Numerical methods employed in various investigations include distribution of Stokeselets, potential sources (Dabros 1985) and spherical singularities combined with the collocation technique (Yuan and Wu 1987; Keh and Tseng 1994) and boundary integral method (Hsu and Ganatos 1989; Gavze 1990b).

In this work an efficient method for calculating forces acting on particles placed in Stokes' flow fields is proposed. The technique is a variant of the boundary integral method used by Hsu and Ganatos (1989) albeit modified by application of the reciprocal theorem (Happel and Brenner 1983). This procedure reduces by half the amount of computations needed by a direct application of the boundary integral equation. This method is used for calculation of forces and torques acting on prolate spheroidal particles located at various distances and inclined at various angles near a wall. Explicitly, the specific goals of this study are (i) investigate the influence of nonsphericity, characterized by the aspect ratio, on the viscous forces and torques acting on the particles fixed near a wall; (ii) calculate the velocities of inertialess particles; and (iii) propose correlations for the particle forces and torques. These will prove useful in various applications, including computing particle trajectories in various flow conditions.

2. MATHEMATICAL FORMULATION

In this section we derive the set of equations determining the force and torque acting on a rigid body suspended in a flow in the vicinity of a plane wall, and the equations for the velocities of non-inertial particles.

2.1. Integral representation of the flow field

Let Ω be a domain in the half space $x_3 > 0$ enclosed within the boundary Σ composed of a subdomain Σ_1 of the plane $x_3 = 0$ and of $\Sigma_2 = \Sigma_p \cup \Sigma_\infty$, i.e. the particle's surface Σ_p and the boundary Σ_∞. Both Σ_∞ and Σ_1 surround the particle as shown in figure 1.

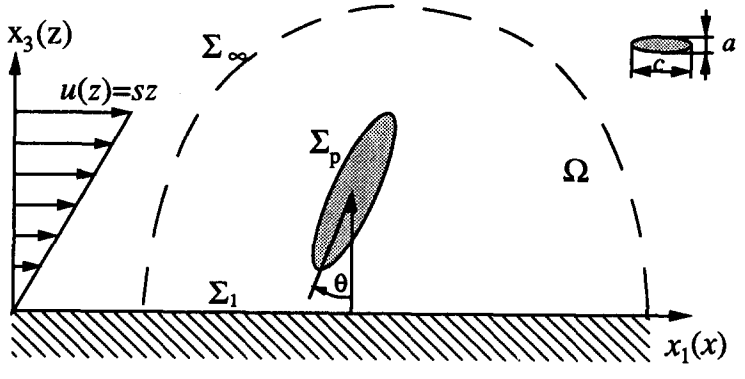

Figure 1. Schematic of a spheroidal particle moving in a shear flow near a solid wall.

Let $(\mathbf{V}, p)$ be any solution of the Stokes equations in Ω with the velocity components V_i vanishing on Σ_1

$$\mu \Delta V_i = \frac{\partial p}{\partial x_i}, \quad \frac{\partial V_j}{\partial x_j} = 0, \quad V_i|_{\Sigma_1} = 0, \quad i = 1, 2, 3. \tag{1a,b,c}$$

Then using the integral representation of the solution of Stokes equation (Ladyzhenskaya 1963) one can express $\mathbf{V} = V_k \mathbf{e}_k$ in the following form

$$V_k = \int_{\Sigma_1 \cup \Sigma_2} U_{ki}(\mathbf{x}, \mathbf{y}) \sigma_{ij}(\mathbf{V}, p) n_j \, d\mathbf{y} - \int_{\Sigma_2} V_i \sigma_{ij}(\mathbf{U}_k, q_k)(\mathbf{x}, \mathbf{y}) n_j \, d\mathbf{y}. \tag{2}$$

The second integral in the r.h.s. of [2] vanishes on Σ_1 due to the boundary condition [1c].

In formula [2] $(\mathbf{U}_k, q_k)$ is the fundamental solution for the velocity and pressure of the Stokes equations in the *infinite unbounded* space:

$$U_{ki}(\mathbf{x}, \mathbf{y}) = \frac{1}{8\pi\mu}\left[\frac{\delta_{ki}}{|\mathbf{x} - \mathbf{y}|} + \frac{(x_k - y_k)(x_i - y_i)}{|\mathbf{x} - \mathbf{y}|^3}\right], \tag{3a}$$

$$q_k(\mathbf{x}, \mathbf{y}) = \frac{1}{4\pi} \frac{y_k - x_k}{|\mathbf{x} - \mathbf{y}|^3}. \tag{3b}$$

That is $U_{ki}(\mathbf{x}, \mathbf{y})$ is the kth component of the velocity at a point $\mathbf{x}$ due to a unit force applied at a point $\mathbf{y}$ in the jth direction. In addition, $|\mathbf{x} - \mathbf{y}|$ is Euclidean distance between the points $\mathbf{x}$ and $\mathbf{y}$ and σ_{ij} is the stress tensor operator

$$\sigma_{ij}(\mathbf{V}, p) = \mu\left(\frac{\partial V_i}{\partial x_j} + \frac{\partial V_j}{\partial x_i}\right) - \delta_{ij} p, \tag{4}$$

where μ is the viscosity. $U_{ij}(\mathbf{x}, \mathbf{y})$ and $\sigma_{ij}(\mathbf{U}_k, q_k)$ appearing in [2] are the kernels of the single- and double-layer potentials (Ladyzhenskaya 1963), with the latter given by

$$\sigma_{ij}(\mathbf{U}_k, q_k) = \frac{3}{4} \frac{(x_i - y_i)(x_j - y_j)(x_k - y_k)}{|\mathbf{x} - \mathbf{y}|^5}. \tag{5}$$

Equation [2] involves integration on both Σ_1 (a subdomain of the plane $x_3 = 0$) and Σ_2. It can be simplified to involve only integration on Σ_2 by introduction of the Green's function for the half space $x_3 \geqslant 0$ (Blake 1971). The Green's function consists of a velocity tensor field $G_{ki}(\mathbf{x}, \mathbf{y})$ and a pressure vector $g_k(\mathbf{x}, \mathbf{y})$. The pair $(\mathbf{G}, \mathbf{g})$ satisfies the Stokes equation in the half space $x_3 > 0$ and the boundary condition

$$(U_{ki} + G_{ki})\Big|_{\substack{x_3 = 0 \\ y_3 > 0}}^{} = (U_{ki} + G_{ki})\Big|_{\substack{y_3 = 0 \\ x_3 > 0}}^{} = 0. \tag{6}$$

Thus, for every $\mathbf{V}$ and p satisfying the Stokes equations in Ω and vanishing on Σ_1 an alternative representation is obtained with the aid of the reciprocal theorem (Happel and Brenner 1983)

$$V_k(\mathbf{x}) = \int_{\Sigma_2} [U_{ki}(\mathbf{x}, \mathbf{y}) + G_{ki}(\mathbf{x}, \mathbf{y})] \varphi_i(\mathbf{y}) d\mathbf{y} - \int_{\Sigma_2} V_i \sigma_{ij}(\mathbf{U}_k + \mathbf{G}_k, q_k + g_k) n_j \, d\mathbf{y} \tag{7}$$

(Gavze 1990b; Hsu and Ganatos 1989). Here $\varphi_i (i = 1, 2, 3)$ given by

$$\varphi_i(\mathbf{y}) = \sigma_{ij}(\mathbf{V}, p) n_j \tag{8}$$

are the stress vector components on the surface of the body. In the following we will extend the boundary Σ_∞ to infinity, whereas Σ_1 will become the whole plane $x_3 = 0$. We consider solutions which vanish at infinity so that the integrals over $\Sigma\infty$ in [7] vanish. Equation [7] may be used to

calculate the force and torque acting on a rigid body immersed in any (rather than quiescent) Stokes flow velocity **W** prevailing in the half space $x_3 > 0$ (for example, shear flow).

Suppose a body is moving in the fluid with a translational velocity U_i^b and an angular velocity ω_i^b. Define a Stokes flow field $V_i(\mathbf{x})$ which satisfies the following boundary conditions

$$V_i|_{x_3=0} = 0, \quad V_i|_{\Sigma_p} = U_i^b + \epsilon_{ijk}\omega_j^b x_k - W_i|_{\Sigma_p}, \quad V_i|_{\Sigma_\infty} = 0. \tag{9}$$

The total flow accounting for the presence of the body is given by $\mathbf{V} + \mathbf{W}$. It may be shown, that since the velocity **W** is the solution for the Stokes equations in the half space $x_3 > 0$, it does not contribute to the force and torque, acting on the body. When **x** in [7] tends to the boundary Σ_p, the following equation is obtained for φ_i due to the discontinuity of the double layer potential (Ladyzhenskaya 1963)

$$\tfrac{1}{2}V_k(\mathbf{x}) = \int_{\Sigma_p} [U_{ki}(\mathbf{x}, \mathbf{y}) + G_{ki}(\mathbf{x}, \mathbf{y})]\varphi_i(\mathbf{y})d\mathbf{y} - \int_{\Sigma_p} V_i\sigma_{ij}(\mathbf{U}_k + \mathbf{G}_k, q_k + g_k)n_j \, d\mathbf{y}. \tag{10}$$

Equation [10] is a Fredholm integral equation of the first kind for the unknown stresses φ_i. The velocity V_i on Σ_p is given in [9]. In the above notation **n** is the outer normal to Ω, i.e. the inner normal to the body so that φ_i are the stresses that the body exerts upon the fluid.

Equation [10] was used by Hsu *et al.* (1989). It requires the computation of the two integrals in the r.h.s. of [10].

2.2. *The reciprocal theorem method (r.t.m.)*

The reciprocal theorem enables to apply an alternative procedure in which only computation of the single layer potential is needed. The method is based on the choice of some basic flow fields and application of the reciprocal theorem on these fields and the field **V** [9] (Karrila and Kim 1989; Gavze 1990a).

Define the "basic solutions" $(\mathbf{V}^k, p^k)$ and $(\mathbf{W}^k, q^k)$ which satisfy the Stokes equations [1] in Ω, subject to the following boundary conditions

$$V_i^k|_{\Sigma_p} = \delta_{ik}, \quad V_i^k|_{x_3=0} = 0, \quad V_i^k|_{\Sigma_\infty} = 0, \tag{11a}$$

$$W_i^k|_{\Sigma_p} = \epsilon_{ijl}\delta_{kj}x_l = \epsilon_{ikl}x_l, \quad W_i^k|_{x_3=0} = 0, \quad W_i^k|_{\Sigma_\infty} = 0. \tag{11b}$$

$(\mathbf{V}^k, p^k)$ is the flow field caused by the translation of the particles in the kth direction in a quiet fluid, $(\mathbf{W}^k, q^k)$ is the flow field caused by its rotation in the kth direction. In the following we will denote the stresses on Σ_p by

$$\phi_i^k = \sigma_{ij}(\mathbf{V}^k, p^k)n_j|_{\Sigma_p}, \quad \psi_i^k = \sigma_{ij}(\mathbf{W}^k, q^k)n_j|_{\Sigma_p}, \tag{12}$$

where ϕ_i^k, ψ_i^k are the ith component of the stress due to translation and rotation in the kth direction, respectively.

Define the translation, coupling and rotation tensors, **K**, **C**, $\boldsymbol{\Omega}$ in the same way as for an unbounded fluid (Happel and Brenner 1973), with the exception that in the present circumstances they depend on the particle's distance from the wall and its orientation

$$K_{ik} = -\int_{\Sigma_p} \phi_i^k \, d\mathbf{y}, \tag{13a}$$

$$C_{ik} = -\epsilon_{iml}\int_{\Sigma_p} y_m\phi_l^k \, d\mathbf{y} = -\int_{\Sigma_p} \psi_k^i \, d\mathbf{y}, \tag{13b}$$

$$\Omega_{ik} = -\int_{\Sigma_p} \epsilon_{iml}y_m\psi_l^k \, d\mathbf{y}. \tag{13c}$$

$\mathbf{K}$ and $\mathbf{\Omega}$ are symmetric tensors, which property and the equality between the two expressions of C_{ik} in [13b] follow from the reciprocal theorem (Happel and Brenner 1983).

We will further provide expressions for the force and the torque acting on a particle placed in an arbitrary Stokes' flow, the velocity of which vanishes on $x_3 = 0$. Applying the reciprocal theorem to the flow velocities V_i and V_i^k given by [9] and [11a], respectively, we get

$$\int_{\Sigma_p} V_i \sigma_{ij}(\mathbf{V}^k, p^k) n_j \, d\mathbf{y} = \int_{\Sigma_p} V_i^k \sigma_{ij}(\mathbf{V}, p) n_j \, d\mathbf{y}. \qquad [14]$$

After substitution of the boundary conditions [11], [9] the r.h.s. of [14] yields the force component f_k

$$\int_{\Sigma_p} V_i^k \sigma_{ij}(\mathbf{V}, p) n_j \, d\mathbf{y} = \delta_{ik} \int_{\Sigma_p} \sigma_{ij}(\mathbf{V}, p) n_j \, d\mathbf{y} = f_k,$$

and the l.h.s. will be

$$\int_{\Sigma_p} V_i \sigma_{ij}(\mathbf{V}^k) n_j \, d\mathbf{y} = \int_{\Sigma_p} (-W_i + U_i^b + \epsilon_{ilm} \omega_l^b y_m) \phi_i^k \, d\mathbf{y} = -\int_{\Sigma_p} W_i \phi_i^k \, d\mathbf{y} - U_i^b K_{ik} - \omega_l^b C_{lk}.$$

Therefore, the force exerted on the body is given by

$$f_k = -\int_{\Sigma_p} W_i \phi_i^k \, d\mathbf{y} - U_i^b K_{ik} - \omega_l^b C_{lk}. \qquad [15]$$

In the same manner we get the expression for the torque components

$$t_k = -\int_{\Sigma_p} W_i \psi_i^k \, d\mathbf{y} - U_i^b C_{ki} - \omega_i \Omega_{ik}. \qquad [16]$$

A more general version of these relations, valid for unsteady flows in an unbounded fluid is given in Gavze (1990a). Equations [13], [15] and [16] show that the only unknown in the expressions for f_k and t_k are the surface stresses of the six basic solutions [11]. These stresses may be obtained by solving integral equation [10]. Basing on the discontinuity of the double layer potential (Ladyzhenskaya 1963) it may be easily shown that for $\mathbf{x} \in \Omega$ the double layer potential term, i.e. the second integral in the r.h.s. of [7], vanishes for any solution $(\mathbf{V}, p)$ which on the particle surface Σ_p yields the rigid body velocity. In particular, it vanishes upon substituting $(\mathbf{V}^k, p^k)$ and $(\mathbf{W}^k, q^k)$ in place of $(\mathbf{V}, p)$. Using this and the continuity of the single layer potential one can pass to the limit $\mathbf{x} \to \Sigma_p$ to obtain the following set of equations for ϕ_i^k and ψ_i^k

$$V_i^k|_{\Sigma_p} = \delta_{ik} = \int_{\Sigma_p} [U_{ij}(\mathbf{x}, \mathbf{y}) + G_{ij}(\mathbf{x}, \mathbf{y})] \phi_j^k \, d\mathbf{y} \quad \mathbf{x} \in \Sigma_p, \qquad [17a]$$

$$W_i^k|_{\Sigma_p} = \epsilon_{ikl} x_l = \int_{\Sigma_p} [U_{ij}(\mathbf{x}, \mathbf{y}) + G_{ij}(\mathbf{x}, \mathbf{y})] \psi_j^k \, d\mathbf{y} \quad \mathbf{x} \in \Sigma_p. \qquad [17b]$$

Further we will change the notation of the Cartesian components $(x_1, x_2, x_3) \to (x, y, z)$ and of the velocity components $(u_1, u_3, \omega_2) \to (u, w, \omega)$.

2.3. *Numerical solution*

Calculations were performed for prolate spheroids, whose axes of symmetry lie in the x–z plane. Denote by θ the angle between the particle's symmetry axis and the z-axis (see figure 1). The surface of the particle was divided into elements, each of which consists of several flat triangles which have

Table 1. Comparison between numerical and analytical results of Jeffery (1922) for spheroids in a shear flow far from the wall $\theta = 0.25\pi$

	$F_x/\mu csz$		$F_z/\mu csz$		$T_y/\mu c^3 s$	
a/c	Numer.	Analyt.	Numer.	Analyt.	Numer.	Analyt.
0.1	6.055	6.088	− 1.088	− 1.098	1.661	1.680
0.2	7.798	7.834	− 1.106	− 1.105	2.310	2.333
0.35	10.027	10.079	− 1.002	− 0.999	3.361	3.398
0.5	12.105	12.172	− 0.827	− 0.825	4.670	4.728
0.7	14.789	14.872	− 0.530	− 0.529	7.026	7.124
0.8	16.113	16.204	− 0.363	− 0.362	8.536	8.660
0.9	17.432	17.529	− 0.186	− 0.185	10.309	10.464
0.95	18.089	18.190	− 0.095	− 0.094	11.304	11.476
0.99	18.614	18.718	− 0.021	− 0.019	12.155	12.342
0.9999	18.744	18.848	− 0.002	− 0.000	12.373	12.564
0.999999	18.747	18.850	− 0.000	− 0.000	12.434	12.567

their vertices on the actual surface of the body. In the present case we used 1200 triangles comprising 312 elements. The Galerkin method was used to solve [17a,b] with constant base functions. System [17] reduces to a finite set of algebraic equations of the form

$$[\tilde{\mathbf{U}} + \tilde{\mathbf{G}}]\cdot\tilde{\phi} = \mathbf{V}^0 \qquad [18]$$

for the unknown vector $\tilde{\phi}$, with the latter and the matrices $\tilde{\mathbf{U}}$,$\tilde{\mathbf{G}}$ being discrete forms of their corresponding continuous counterparts, appearing in [17] and $\mathbf{V}^0$ standing either for $\mathbf{V}^k$ or $\mathbf{W}^k$ ($k = 1, 2, 3$). The matrix $\tilde{\mathbf{U}} + \tilde{\mathbf{G}}$ is symmetric positive definite, and, therefore, system [18] may be solved by any standard computational procedure, even though, the matrix condition number is normally large (Gerald and Wheatley 1989). The matrix $\tilde{\mathbf{U}}$ corresponds to the particle's motion in an unbounded fluid and has, therefore, to be calculated only once. The matrix $\tilde{\mathbf{G}}$ depends on the location and orientation relative to the plane $z = 0$. Most of the computation time is spent on constructing the matrix $\tilde{\mathbf{G}}$; therefore, the use of [17] instead of [10] saves approximately 50% of the computation time. A more detailed description of the discretization of the equations is given in Gavze (1990b).

The reciprocal theorem method (r.t.m.), when applied to different spheroids in the unbounded quiet fluid results in errors of about 0.5% for the translation tensor $\mathbf{K}$ and of 1–2% for the rotation tensor $\boldsymbol{\Omega}$. We also compare the data obtained by the r.t.m. with the analytical results of Oberbeck (see Happel and Brenner 1983; Jeffery 1922; etc.) for prolate spheroids in an unbounded shear flow for aspect ratios ranging from 0.1 to 0.999999 (see table 1). The errors for F_x and F_z are generally less than 1% except for F_z for aspect ratio very close to 1, where the analytical results approach zero faster than the numerical data. For T_y the error is no more than 1.5%.

In table 2 we compare the force F_x and the torque T_y acting on a sphere in a shear flow near a wall with the analytical solution (Goldman *et al.* 1967b). The error in F_x is less than 1% and in T_y is less than 1.5%. The free velocities u and ω of inertialess spherical particles, are also compared in table 2 with the analytical solution of Goldman *et al.* (1967b). For particle–wall

Table 2. Comparison with the analytical solution of Goldman *et al.* (1967b) for spherical particles in a shear flow near a wall. Free translational (u) and rotational (ω) velocities of inertialess particles. Force (F_x) and torque (T_y) acting on fixed spherical particles

	u/as		ω/s		$F_x/6\pi\mu asz$		$T_y/4\pi\mu a^3 s$	
z/a	Numer.	Analyt.	Numer.	Analyt.	Numer.	Analyt.	Numer.	Analyt.
1.0453	0.699	0.683	0.350	0.337	1.654	1.668	0.935	0.948
1.1276	0.871	0.865	0.396	0.390	1.603	1.616	0.941	0.954
1.5431	1.425	1.423	0.465	0.462	1.428	1.439	0.961	0.974
2.3524	2.301	2.300	0.492	0.489	1.269	1.278	0.977	0.990
3.7622	3.741	3.741	0.500	0.497	1.159	1.167	0.984	0.997
10.0677	10.064	10.064	0.502	0.500	1.052	1.059	0.987	1.000

(normalized) gap of 0.0453 the error is 3–4%, but for a gap width of 0.1276 it already reduces to less than 1.5%. In appendix A we present for the sake of convenience analytical solutions for $\mathbf{K}$, $\mathbf{\Omega}$, F_x, F_z, T_y, u, ω in an unbounded fluid.

3. RESULTS

3.1. Forces and torques in a shear flow

Lift force. Figure 2 presents the z-component of the force (F_z) acting on a particle perpendicular to the flow direction (lift force). This force is antisymmetric with respect to $\theta = \pi/2$, which may be proven from [1a–c] by inverting the flow direction or changing s by $-s$. The maximum force is attained at the angle $\theta = \pi/4$, similarly to the case of free shear flow (see [A13]). The influence of the wall proximity is to increase this maximum (see figure 2(b)). However, this effect depends on the particle aspect ratio and is most pronounced for spheroids with $a/c \sim 0.35$. This means that the effect of the wall on F_z for $\theta = \pi/4$ is weak both for oblong particles ($a/c \ll 1$) and for particles whose shape approaches to spherical ($a/c \approx 1$. This nonmonotonic dependence of F_z upon a/c may be rationalized by noting that spherical particles experience no lift. On the other hand, with increasing nonsphericity (decreasing a/c) the major part of the particle extends far from the wall, where almost free shear flow (i.e. undisturbed by the wall-particle interactions) prevails. Therefore, the wall effect is the strongest for moderate nonsphericities.

The above conclusion drawn for $\theta = \pi/4$ is also valid for other angles, excluding $\theta = 0$ and $\pi/2$. At these angles F_z vanishes due to the linearity of the governing equations [1] and geometrical symmetry with respect to z-axis. As a rule of thumb, the effect of the wall extends to the distance of about 5–10 shorter axes, beyond which it may be neglected with the error not exceeding 2–5%.

The lift force discussed here is a pure viscous force resulting from the combined effect of particle nonsphericity and the wall effect. It should not be mixed with other lift forces, arising from the flow inertia (Saffman 1965).

Drag force F_x. An expression for the drag force, which is the component of the viscous force parallel to the flow direction in the unbounded flow (F_x^∞) is given in [A13]. The effect of the wall is to increase this force with respect to the free shear flow due to no-slip condition imposed on the wall surface. This may be seen in figure 3, showing the difference $\Delta F_x = F_x - F_x^\infty$ for $\theta = 0$. The latter difference, called here "wall induced drag force" is less for spheroids (at any orientation) than for spherical particles. For spherical particles one can calculate ΔF_x using the expression (Faxen 1923; Happel and Brenner 1983):

$$\frac{F_x}{F_x^\infty} = \frac{1}{1 - 9c/(16z)} + O(c/z)^3, \quad (a/c = 1),$$

where $F_x^\infty = 6\pi\mu csz$. The above expression may be used to express

$$F_x - F_x^\infty = \frac{9}{16}\frac{6\pi\mu sc^2}{1 - 9c/(16z)} + O(c/z)^2, \quad (a/c = 1, c/z \to 0). \qquad [19]$$

The wall induced drag force ΔF_x diminishes with decreasing aspect ratio a/c. This accords with a similar trend exhibited by the lift force. Generally, with the longer axis c and z/c fixed, the perturbation which a spheroid exerts on the flow diminishes with decreasing a. Consequently, all particle–wall hydrodynamic interactions diminish with decreasing particle minor axis.

One striking feature of the wall induced drag force is that it is relatively independent of the particle distance from the wall. As shown above, this effect is most pronounced for oblong particles. On the other hand, ΔF_x does not vanish for $z/c \to \infty$ (see [19]). To rationalize this result, imagine a spherical particle moving with a speed U in an otherwise stagnant fluid, bounded by a solid wall. The particle experiences a force $F_x = 6\pi\mu cU + \Delta F$, where the perturbation ΔF introduced by the wall decays as $1/z$. In our case we have a particle *fixed in a shear flow*, i.e. its relative velocity

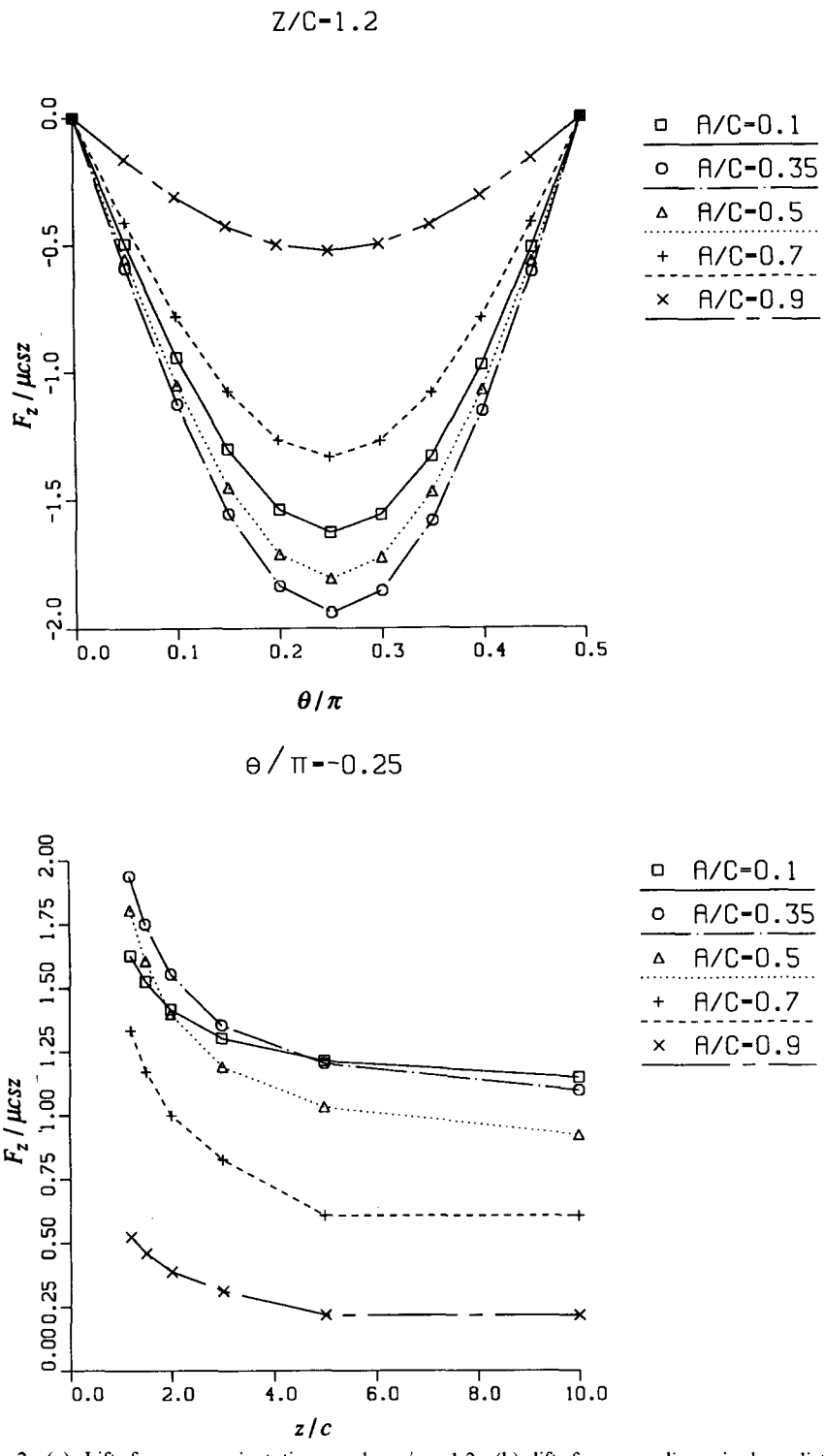

Figure 2. (a) Lift force vs orientation angle, $z/c = 1.2$; (b) lift force vs dimensionless distance, $\theta/\pi = -0.25$.

$U(z) = sz$ with respect to the local flow velocity increases proportionally to z. Hence the perturbation of the force is of order $O(1/z)U(z) = O(1)$ (see [19]).

In close vicinity to the wall $z/c \to 0$, one can use the lubrication theory to show for the sphere that (Goldman 1967b)

$$F_x - F_x^{\infty} = 0.7005 \times 6\pi\mu sc^2 \quad (a/c = 1, z/c \to 0). \qquad [20]$$

Therefore, the variation with z/c of the wall induced drag force is

$$0.5625 < \frac{F_x - F_x^\infty}{6\pi\mu sc^2} < 0.7005 \quad (a/c = 1), \qquad [21]$$

which is less than $\pm 11\%$. This variation gives an upper bound for the comparable quantity of spheroids.

Torque T_y. Figure 4 presents the normalized difference ΔT_y between the torques calculated in the vicinity of the wall and in the unbounded flow ($z/c = \infty$). Clearly, ΔT_y depends on the particle orientation angle θ. Figure 4(a) shows that for the majority of orientations and aspect ratios the wall tends to reduce the torque. The effect of the wall on the flow near a spheroid with its longer axis oriented parallel to the wall ($\theta = \pi/2$) is to slow down the flow in the gap between the particle and the wall, and hence to reduce the viscous friction in "lower" (i.e. facing the wall) side of the particle. Hence such a particle experiences a larger torque than its counterpart in a free shear flow.

A particle fixed in an upright position (perpendicular to the flow) experiences a torque which stems form the flow speed up around its surface. The effect of the wall on the flow near a spheroid fixed in such a position ($\theta = 0$) is to slow down the fluid motion along the particle surface in the z direction. Hence the speed up of the flow over the upper particle edge is weaker, which results in the concomitant reduction of the skin friction. Accordingly, such a particle experiences a smaller torque than T_y^∞. These qualitative considerations are confirmed by the data shown in figure 4(b) for $a/c = 0.2$. The most dramatic influence of the wall is observed for the smallest distance $z/c = 1.1$. For $\theta = \pi/2$ the effect of the wall is to increase the torque up to 50%. For intermediate orientations (about $\theta/\pi = 0.3$) the above two factors balance each other which results in a weak z-dependence of T_y.

The wall effect on the torque is found to diminish with the aspect ratio approaching unity, i.e. when the particle shape approaches to spherical. This agrees with the results of Goldman (1967b) who showed that the torque acting on a stationary sphere is almost unaffected by the proximity of a solid wall. In particular, when the sphere touches the wall, the torque is reduced by about

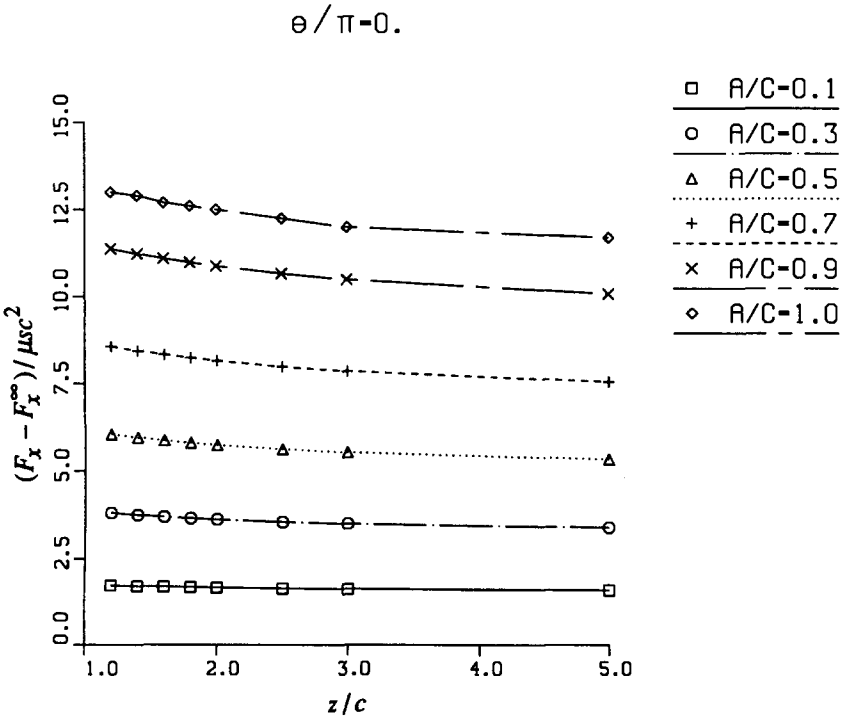

Figure 3. Wall-induced parallel (drag) force, $\theta = 0$.

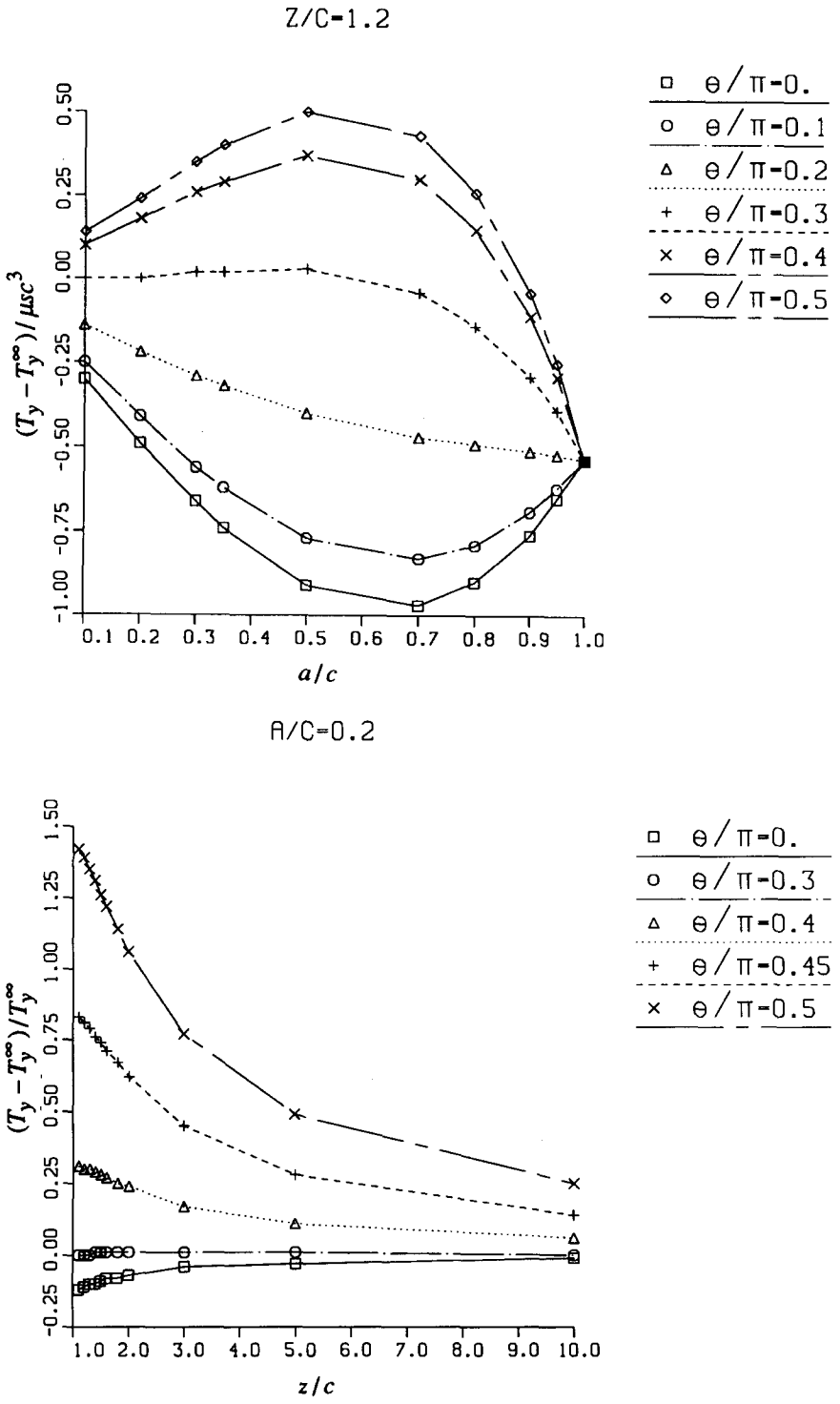

Figure 4. (a) Wall-induced torque vs aspect ratio, $z/c = 1.2$; (b) wall-induced torque vs distance, $a/c = 0.2$.

5.6% with respect to its free stream value ($4\pi\mu sc^3$). At large distances the wall effect for spheres decays as

$$\frac{T_y - T_y^\infty}{T_y^\infty} \approx -\frac{3}{16}(c/z)^3, \quad z \gg c. \qquad [22]$$

A similar decay rate is also observed for spheroids. This is in contrast to the wall induced drag force which does not vanish as $z \to \infty$.

3.2. *Friction coefficients of nonspherical particles in a quiet fluid near a wall*

Some of the components of the friction tensor **K** of spheroidal particles near the wall were studied by Happel and Brenner (1983) and by Hsu and Ganatos (1989). Analytical results were obtained for spherical particles by Goldman *et al.* (1967a, b). Some of these components are presented in figure 5(a)–(c) for $\theta = 0$. One can generally observe that the effect of the wall is to increase the friction tensor components. Secondly, the wall effect decreases with decreasing aspect ratio, i.e. spherical particles are mostly influenced by the wall proximity. Both of these conclusions are consistent with those drawn above for the forces acting on particles fixed in a shear flow.

Figure 6 presents the ratio K_{xz}/K_{xz}^{∞} as a function of the aspect ratio a/c, for $z/c = 1.2$ and several orientations. The plot shows a marked z/c-dependence of K_{xz}/K_{xz}^{∞} which for nearly spherical particles $a/c = 0.95$ and $z/c = 1.2$ leads to about six-fold increase of the relative force with respect to the oblong particles of $a/c = 0.1$. On the other hand, the dependence of K_{xz}/K_{xz}^{∞} on the orientation angle θ is weak, which is used in constructing the appropriate correlation (see appendix B). Note also that for spheres $K_{xz} = 0$ for all z.

Figure 7 shows the coupling component C_{yx} of the friction tensor. $-C_{yx}$ is the torque (in the y direction) due to particle translational motion parallel to the wall (in the x-direction) or, equivalently, the parallel drag force induced by the particle rotation. In the unbounded fluid the components of the coupling tensor vanish for ellipsoidal particles. This is no longer true near the wall where they differ from zero, also for spheres (see figure 7(b)). For spheres C_{yx} is negative, since the overall drag on the lower part of the particle (which is closer to the wall) is larger than the drag on the upper part. This is also true for a spheroid the longer axis of which is perpendicular to the wall ($\theta = 0$).

The explicit form of C_{yx} is given by (cf. [13b])

$$C_{yx} = -\int_{\Sigma_p} (z'\phi_x^x - x'\phi_z^x)\mathrm{d}s,$$

where $z' = z - z_0$ and $x' = x - x_0$ are the coordinates relative to the particle center (x_0, z_0) and the quantities ϕ_x^x, ϕ_z^x are the stress components in x-direction generically defined in [12]. For elongated spheroids in upright positions ($\theta = 0$) the second term within the integral is small compared with the first one. The stresses ϕ_x^x act in the direction against the particle motion. They are larger on the side of the particle surface closer to the wall, than on the opposite side. Therefore, the resulting torque acts clockwise, i.e. $C_{yx} < 0$.

For a parallel orientation ($\theta = \pi/2$) C_{yx} of a sufficiently long spheroid is positive, as was observed by Hsu and Ganatos (1989). At this orientation the term $x'\phi_z^x$ is the dominant term in the above expression for C_{yx}. The quantity ϕ_z^x is larger at the particle half surface, which is closer to the wall than at the opposite half. Moreover, ϕ_z^x is positive at the part of the particle surface facing the flow (front side) and negative at the rear side. All this results in a hydrodynamic torque, which acts counterclockwise, i.e. $C_{yx} < 0$.

With decreasing aspect ratio the coupling disappears $C_{yx} \to 0$. This accords with the general effect that the wall exerts on oblong particles. Namely, with decreasing a/c spheroids behave like in a free shear flow (see similar conclusions drawn for F_z and F_x). A competitive influence of the above tendencies yields the most profound θ-dependence of C_{yx} for an intermediate aspect ratio of about $a/c = 0.7$ at which value the $C_{yx}(\gamma)$ curves exhibit minima for $\theta \leqslant 0.2\pi$ and maxima for $\theta \geqslant 0.4\pi$ (see figure 7(a)).

Figure 8 shows the coupling component C_{yz} of the friction tensor. $-C_{yz}$ is the torque caused by particle translation perpendicular to the wall, or the perpendicular lift force arising from particle rotation. It vanishes for spherical particles for all z and for spheroidal particles far from the wall. Moreover, for the latter particles $C_{yz} = 0$ for symmetrical configurations $\theta = 0, \pi/2$. For oblique angles nonzero values of this coefficient stem from the asymmetry of the flow near the particle with

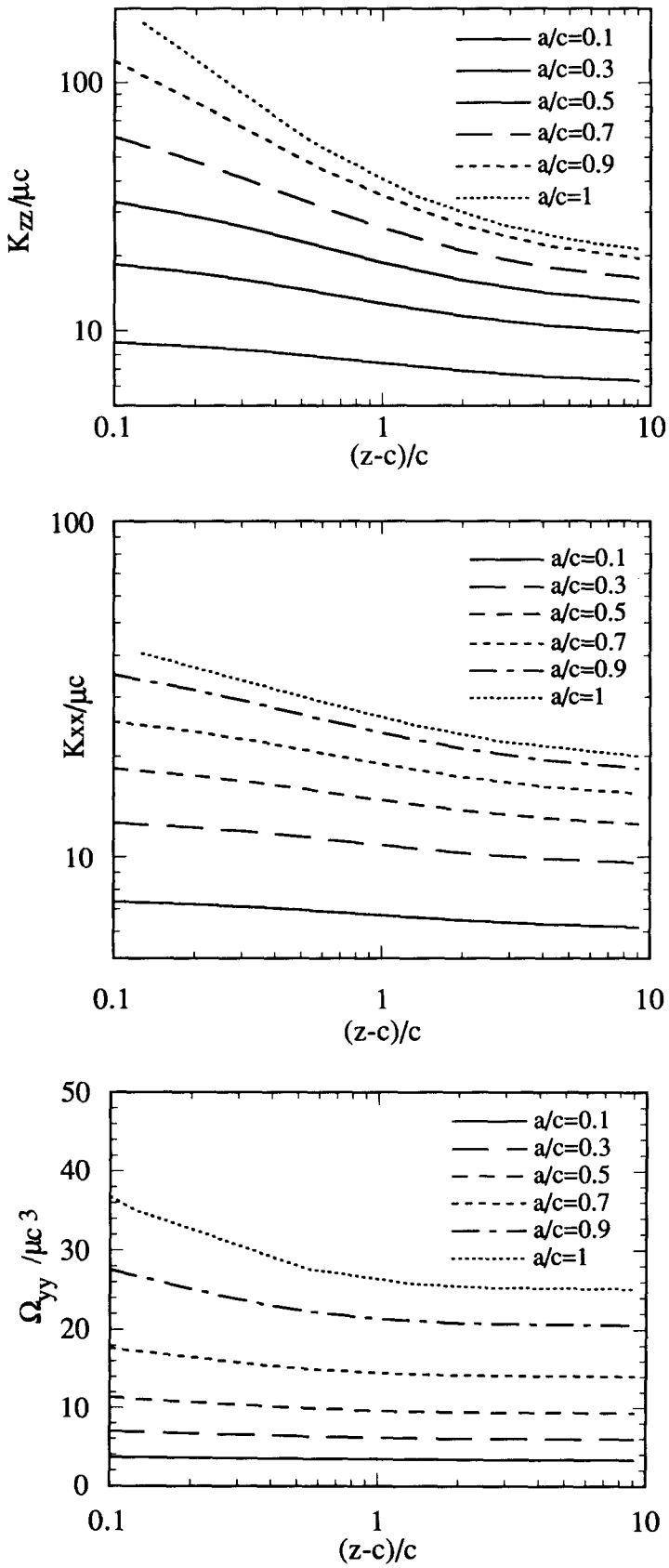

Figure 5. Friction tensor components vs distance $\theta = 0$: (a) lift coefficient; (b) drag coefficient; (c) rotational coefficient.

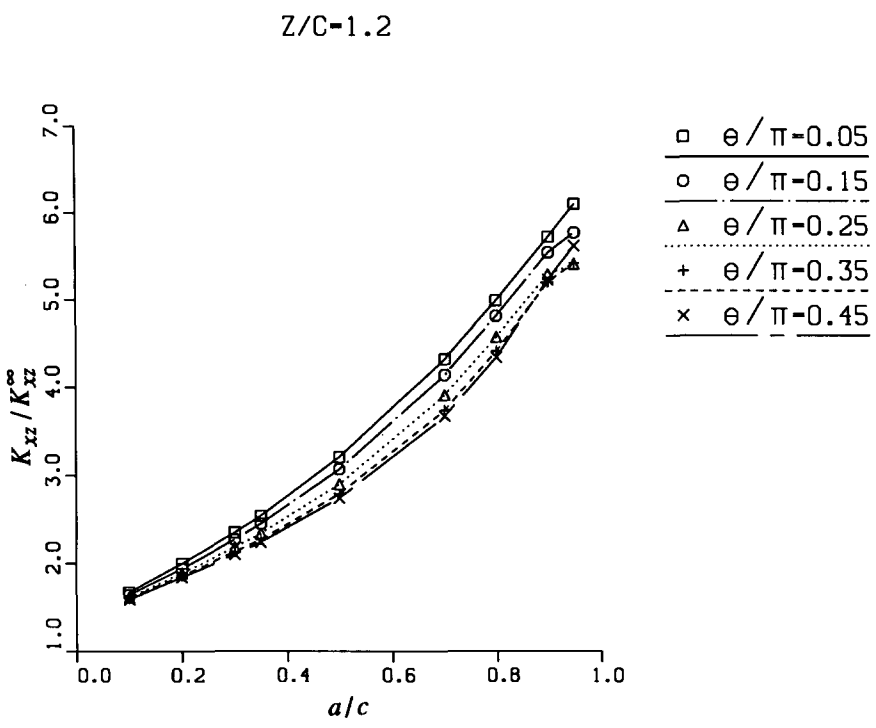

Figure 6. Tensor coupling x–z component.

respect to its short axis. Indeed, the lower part of the spheroid which is closer to the wall, experiences larger drag, than the upper part. This results in a torque acting to align the particle longer axis parallel to the wall. Therefore, a perpendicular orientation ($\theta = 0$) of a spheroid is an unstable one.

The torque caused by particle approaching the wall decays with increasing aspect ratio, as all other hydrodynamic interactions of oblong particles. On the other hand $C_{yz} = 0$ for spheres. A maximum of this coefficient prevails at $a/c \approx 0.7$ (see figure 8). This component causes an unusual kinematic behavior of inertialess nonspherical particles near the wall, analyzed in the next section.

3.3. *Velocities of inertialess particles near the wall*

Here, and in the following, we restrict our consideration to 2D particle motion, i.e. to motion of bodies of revolution whose symmetry axis remains always in the plane x–z. With expressions [15] and [16] at hand we may now write the equation of motion for a particle suspended in a shear flow **W**

$$m\frac{\mathrm{d}u_k}{\mathrm{d}t} = F_k - K_{ik}u_i - C_{2k}\omega_2, \quad k = 1, 3 \qquad [23a]$$

$$\frac{\mathrm{d}}{\mathrm{d}t}(I_{22}\omega_2) = T_2 - \Omega_{22}\omega_2 - C_{2i}u_i, \qquad [23b]$$

where the summation is over the dummy index $i = 1, 3$. Here

$$F_k = -\int_{\Sigma_p} W_i\phi_i^k \,\mathrm{d}\mathbf{y}, \quad T_k = -\int_{\Sigma_p} W_i\psi_i^k \,\mathrm{d}\mathbf{y}. \qquad [24]$$

Assuming that the particle dimensionless relaxation time is small,

$$\tau = \rho_p acs/\mu \ll 1, \qquad [25]$$

where ρ_p is the particle density, one obtains that the terms in the r.h.s. of [23] balance each other. Then one can rewrite [23] in the form

$$\begin{bmatrix} K_{xx} & K_{xz} & C_{yx} \\ K_{zx} & K_{zz} & C_{yz} \\ C_{yx} & C_{yz} & \Omega_{yy} \end{bmatrix} \begin{bmatrix} u \\ w \\ \omega \end{bmatrix} = \begin{bmatrix} F_x \\ F_z \\ T_y \end{bmatrix}. \qquad [26]$$

The matrix in the l.h.s. of [26] is symmetric and positive definite. Therefore, a unique solution for the velocities is always obtainable. These were calculated numerically for various particle aspect ratios, orientations and distances from the wall.

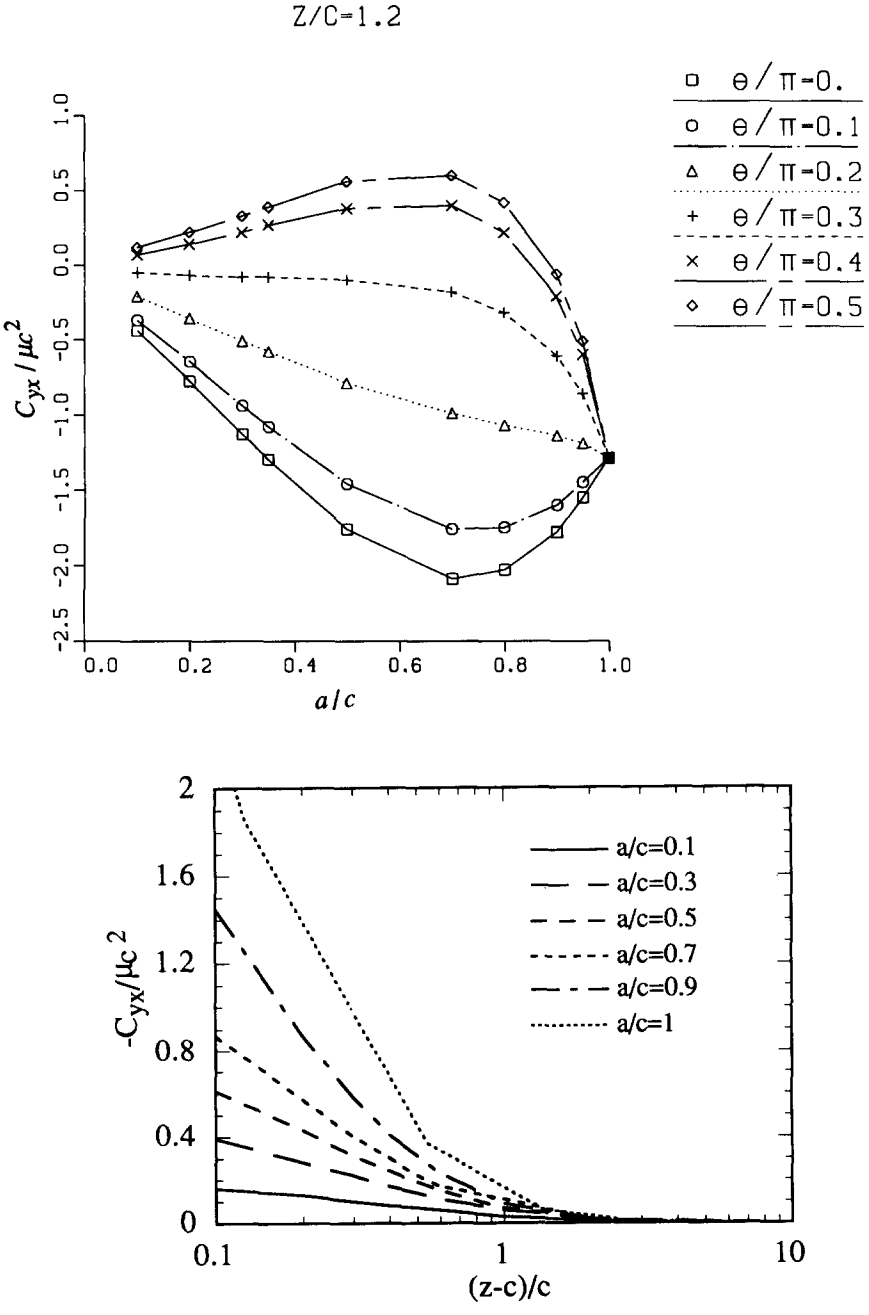

Figure 7. Rotational–translation y–x coupling tensor component (a) vs aspect ratio; (b) vs distance.

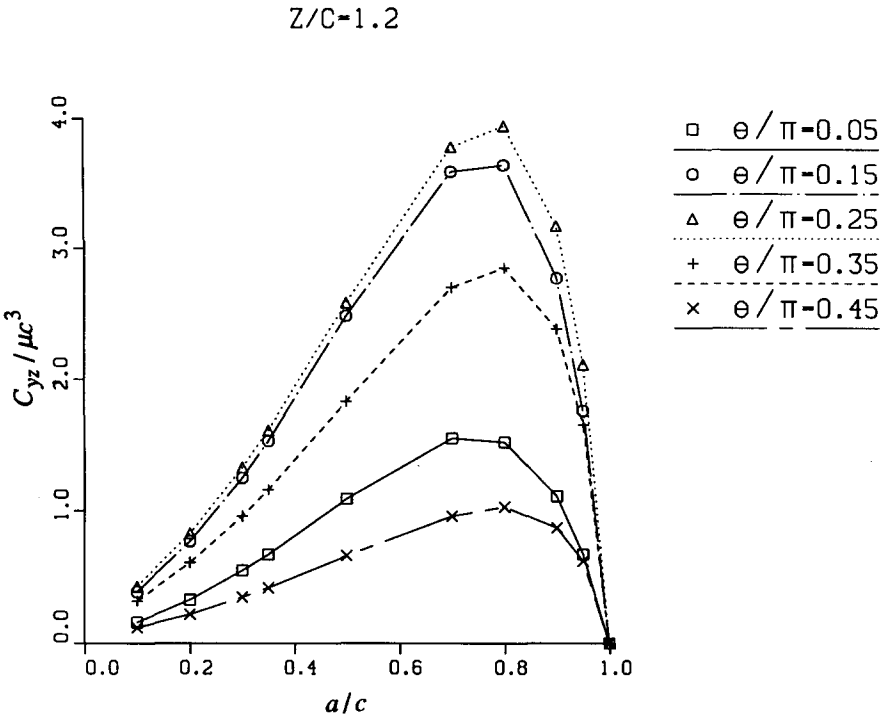

Figure 8. Rotational–translation y–z couupling tensor component vs aspect ratio.

The wall generally tends to increase the particle hydrodynamic interactions. Therefore, particles moving in a shear flow near the wall will have lower velocities than the fluid. This effect was quantified for inertialess neutrally buoyant spherical particles (Goldman *et al.*, 1967b), for which the translational velocity parallel to the wall surface was calculated in the forms:

$$\frac{u}{sz} = 1 - \frac{5}{16}(c/z)^3 + O(c/z)^5, \quad z/c \to \infty, \tag{27a}$$

$$\frac{u}{sz} = \frac{0.7431}{0.6376 - 0.200\ln(z/c - 1)}, \quad z/c \to 1. \tag{27b}$$

Comparable expressions for the angular velocity are:

$$\frac{\omega}{s/2} = 1 - \frac{5}{16}(c/z)^3 + O(c/z)^5, \quad z/c \to \infty, \tag{28a}$$

$$\frac{\omega}{s/2} = \frac{0.8436}{0.6376 - 0.200\ln(z/c - 1)}, \quad z/c \to 1. \tag{28b}$$

The above results imply that the particle translation and rotation are retarded by the wall, whereas its center moves parallel to the wall surface. This is no longer the case for spheroids, which, in addition to the retardation along the flow direction, acquire near a wall a nonzero (lift) velocity component w perpendicular to the wall surface (see figure 9). Unlike the comparable situation in a free shear flow, near the wall translational and rotational motions of spheroidal particles are coupled. This coupling stems from the asymmetry of the flow field prevailing near the spheroid, which results in a vertical (i.e. perpendicular to the wall) motion.

The lift velocity arises from the vertical force F_z and the resistance tensor components $K_{zz}C_{yz}$, shown in figure 8. The lift velocity is an antisymmetric function of θ with respect to $\theta = \pi/2$. It vanishes in all symmetrical configurations ($\theta = 0, \pi/2$) and far from the wall. It reaches a maximum at about $\theta = 0.15\pi$ (see figure 9(a)), where the asymmetry of the flow field near the particle is the

largest. The quantities F_z, K_{xz}, C_{yz} vanish for the spherical form ($a/c = 1$) and so does the lift velocity (see figure 9(a)). In the opposite limite of oblong particles ($a/c \to 0$) the above three quantities approach their unbounded values (see figure 9(b)), thus allowing the only possible solution $w = 0$ of [26].

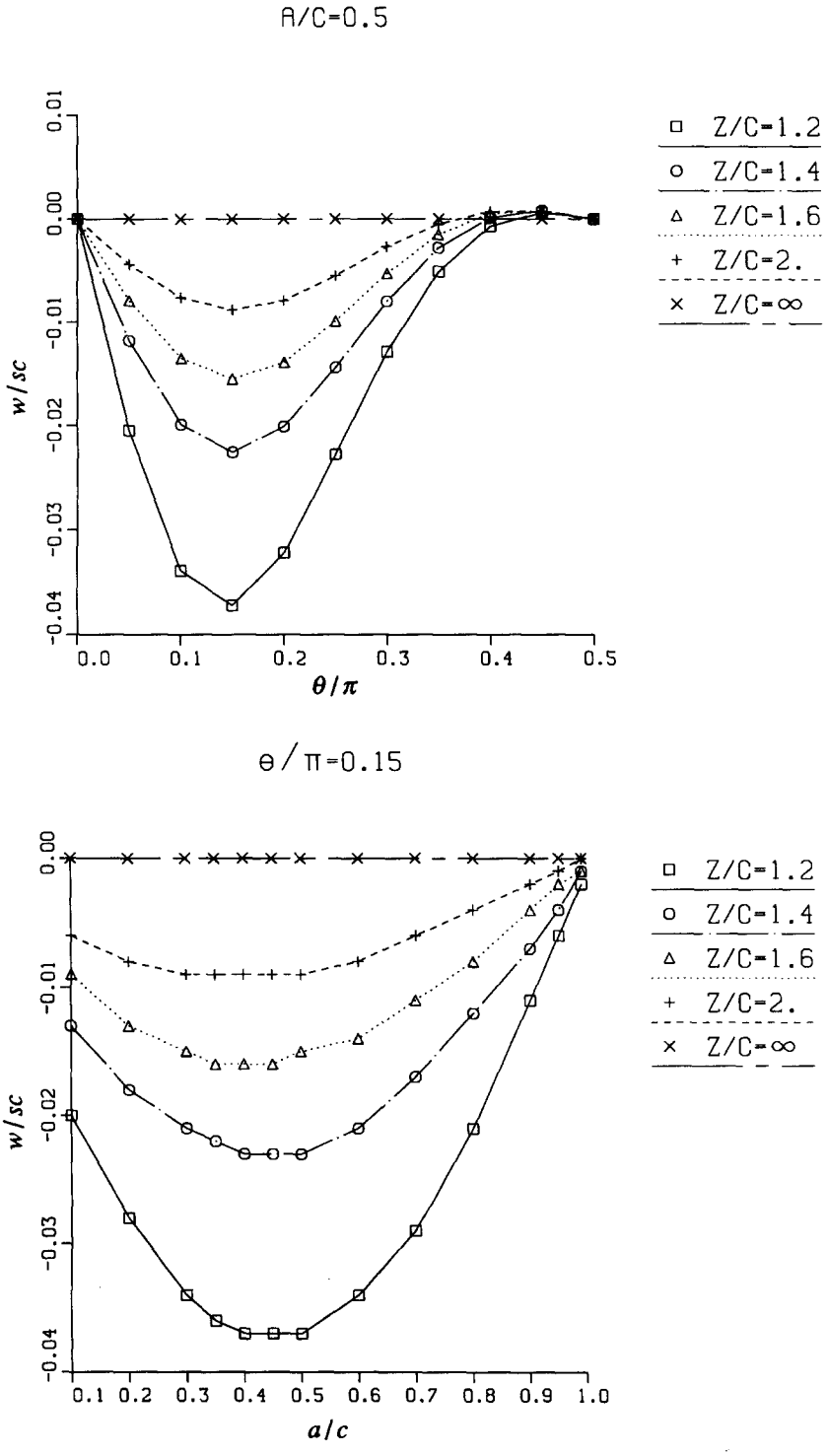

Figure 9. Perpendicular (lift) velocity of inertialess spheroid in a shear flow (a) vs orientation angle; (b) vs aspect ratio.

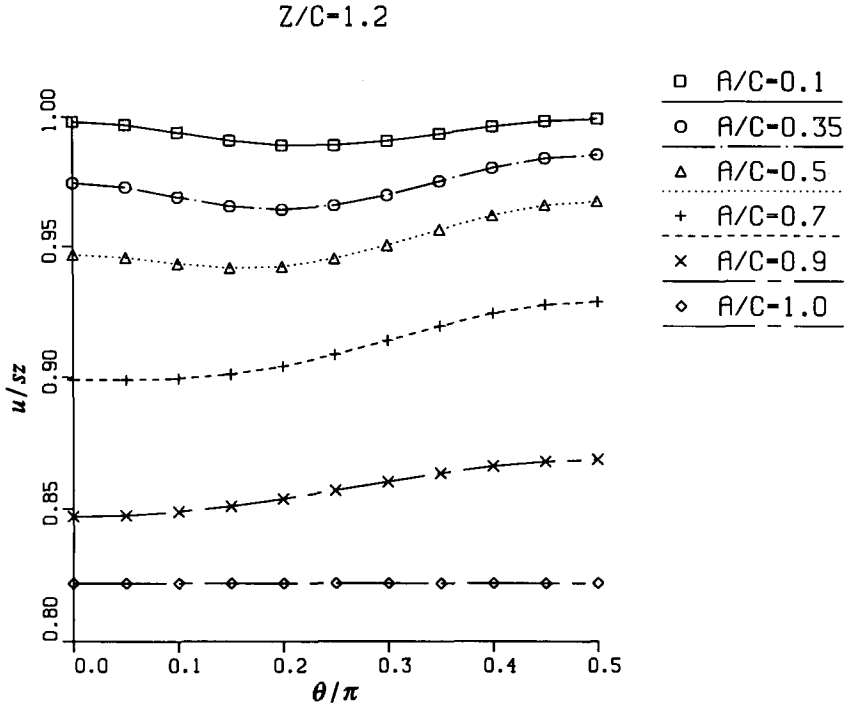

Figure 10. Parallel velocity of inertialess particles vs orientation angle.

Figure 10 presents the normalized horizontal (parallel to the wall) particle velocity component u. One can observe the retardation ($u < sz$), which effect depends weakly on the orientation. It becomes less pronounced with the particle shape deviating from spherical (decreasing a/c), similarly to the behavior of w. This means that the oblong particles succeed to catch up with the flow. In particular, spheroids with $a/c = 0.1$ travel horizontally almost with the local fluid velocity. For $z/c > 2$ the effect of the wall on u amounts to less than 5% for all aspect ratios.

The velocity components u, w both characterize particle drift with respect to the fluid. The effect of orientation on both of these velocity components is shown in figure 11 which presents the vertical velocity w vs the horizontal retardation velocity $u - sz$ for $z/c = 1.2$. The different points on the loop-like curves correspond to different angles ranging between 0 and π. The shift along the horizontal axis in figure 11 from the origin represents the retardation effect. The extensions of the loops along the vertical axes quantify the lift velocity. Clearly the loops plotted for long particles ($a/c = 0.1$) are located about the origin (0,0), since they move with a horizontal velocity close to the flow speed and with vanishing lift velocity. Loops for spherical particles degenerate to points $(u|_{a/c=1} - sz, 0)$ (not shown in figure 11), since in this case the velocity is orientation-independent. As $z/c \to \infty$ all loops shrink to the origin, since there $w = 0$ and $u = sz$.

Angular velocity. Figure 12 depicts the particle angular velocity ω vs the aspect ratio. One can see that the wall weakly affects particle rotation (see figure 12(a)). This is especially true for oblong particles, the motion of which is less influenced by the wall. The retardation effect becomes more pronounced with increasing a/c, and is the strongest for spheres, where the deviation from the free stream angular velocity is still less than about 20%.

For spherical particles $\omega = \text{const}$, i.e. angle-independent. This is no longer true for spheroids, which rotate faster in the perpendicular configuration ($\theta = 0$), since at this point the torque is maximal and the resistance tensor component Ω_{yy} is minimal. The opposite is valid for the parallel configuration ($\theta = \pi/2$), where, therefore, the rotation is the slowest. The angular velocity variations increase with decreasing a/c.

The above a/c-dependence results in the following interesting phenomenon: for each distance there exists an angle θ^*, for which ω does not depend on the particle shape. Clearly, for

$z \to \infty$ $\theta^* = \pi/4$. With approaching the wall θ^* is almost unchanged (increases by about 10%; see figure 12(b)).

An intertialess nonspherical particle in an unbounded shear flow rotates while moving along the streamlines with the rotational period T^∞ (Jeffery 1922; see [A22]). In contrast, a comparable particle released in a shear flow *near a wall* will rotate and move both parallel and perpendicular to the wall. As an integral measure of the particle angular velocity near a wall introduce a period T by integrating $1/\omega$ over all orientations, at a fixed point, i.e.

$$T(z/c, a/c) = \int_0^{2\pi} \omega^{-1}(z/c, a/c, \theta)\mathrm{d}\theta. \qquad [29]$$

Clearly, far from the wall this definition yields T^∞. In fact, the particle will not only rotate with the above period, but also change its distance from the wall, which will obviously yield a rotational period which differs from T. On the other hand, if the particle center is held at $z/c = \text{const}$ it will not perform free rotation, since one has to apply an external force and torque to keep it moving along the streamline. Nevertheless, we will compare the above quantity with T^∞ in order to characterize the cumulative effect of the wall on the particle rotation.

Since the wall slows down the particle rotation the period T increases with decreasing z/c. Far from the wall, T^∞ strongly depends on the aspect ratio a/c and tends to infinity for oblong particles (as $a/c \to 0$, see [A22]). This is due to the fact that a long particle aligned with the flow direction rotates very slowly ($\omega|_{\theta=\pi/2} \to 0$ as $a/c \to 0$; see [A19]). Figure 13 presents the ratio T/T^∞ of the rotational periods: one in the presence of the wall to the one calculated far from the wall, vs distance for various aspect ratios. For $z/c > 1.5$ the wall effect amounts to less than 5%. The wall exerts the strongest influence on those particles whose shape is close to spherical; at $z/c = 1.2$ it constitutes about 25%.

The above conclusions concern the value of the period relative to its unbounded free shear counterpart. Calculations show that particles with $a/c = 0.8$ have the shorter *absolute* rotational periods and those with $a/c = 0.1$ have the longest period.

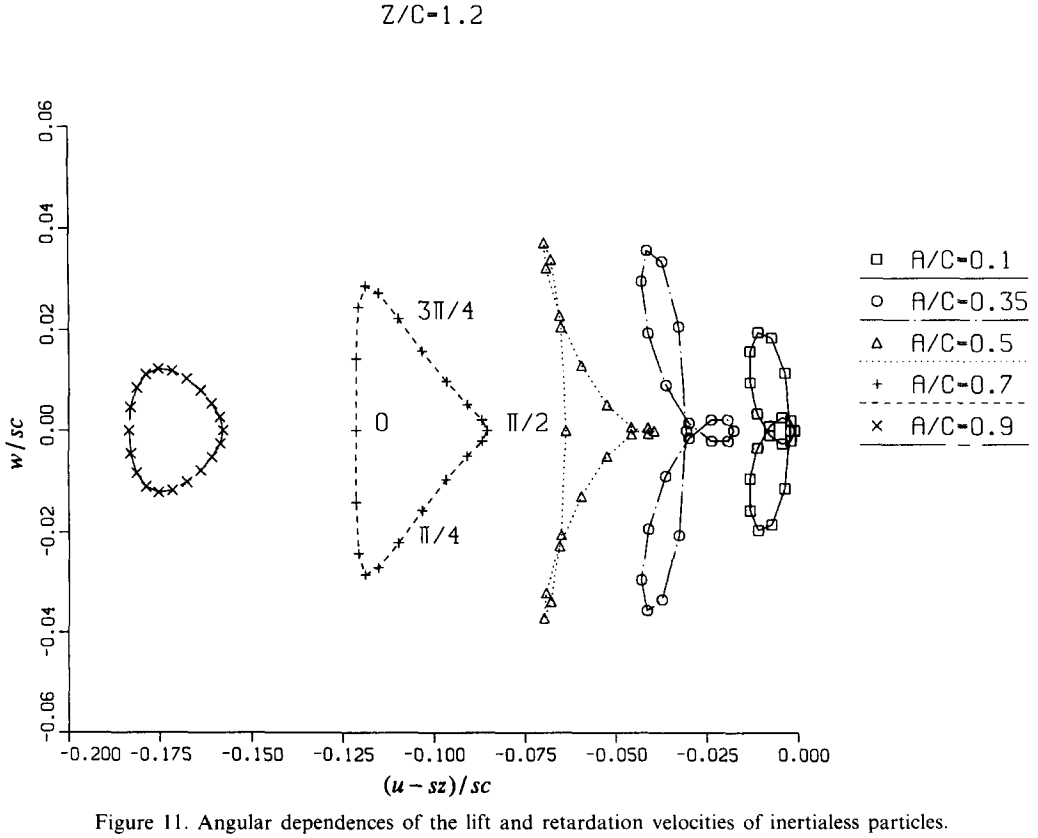

Figure 11. Angular dependences of the lift and retardation velocities of inertialess particles.

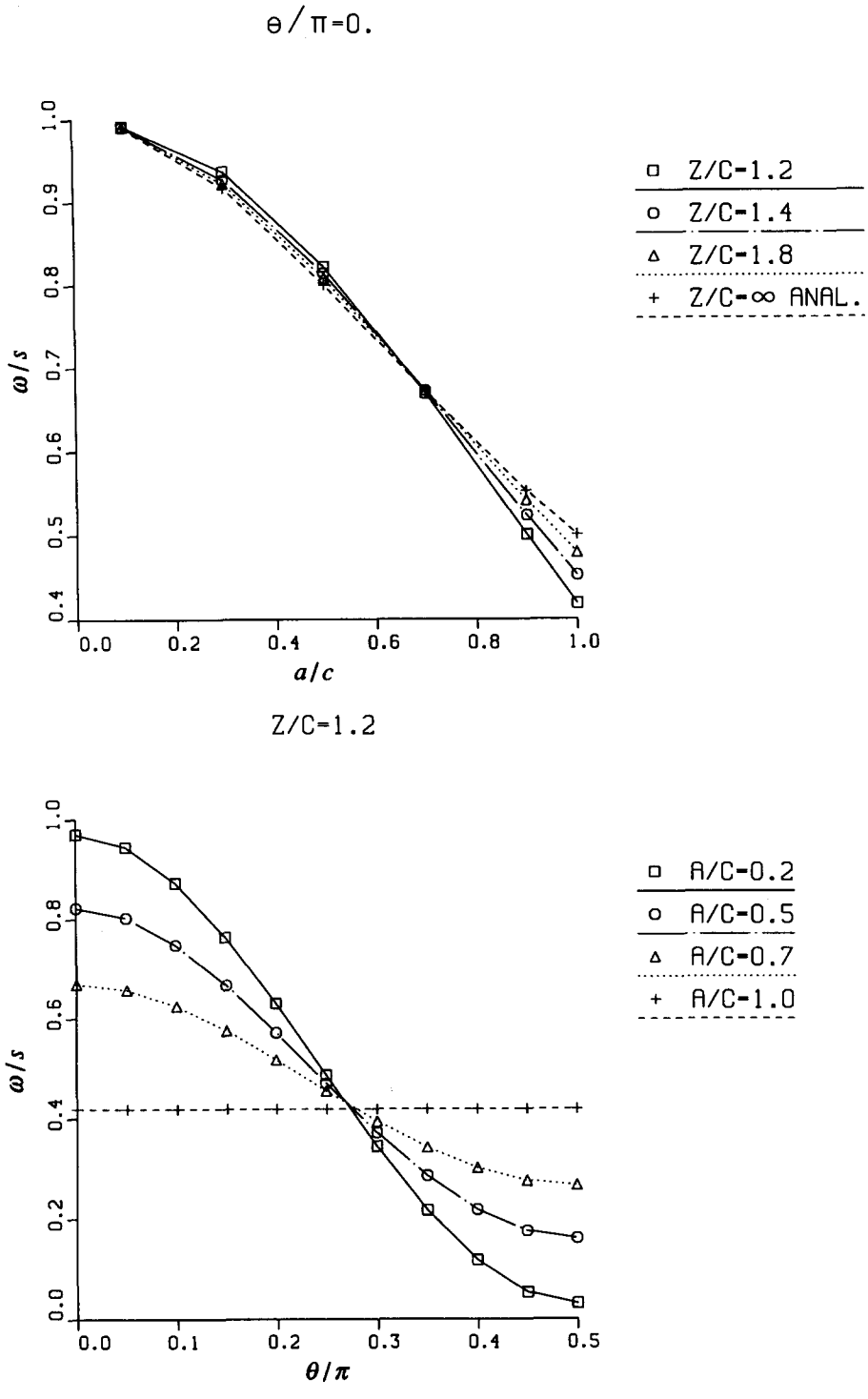

Figure 12. Rotational velocity of inertialess particles (a) vs aspect ratio; (b) vs orientation angle.

These results serve as an indication that the *true* rotational periods of oblong particles, i.e. those accompanied by particle motion perpendicular to the wall, will also be larger than T^{∞}. If the lift velocity w causing this perpendicular motion vanishes in the limit of very long particles, their period T, as defined in [29], has a clear physical meaning. Namely it is the true rotational period of an (oblong) spheroidal particle, the center of which *freely* moves along a streamline parallel to the wall.

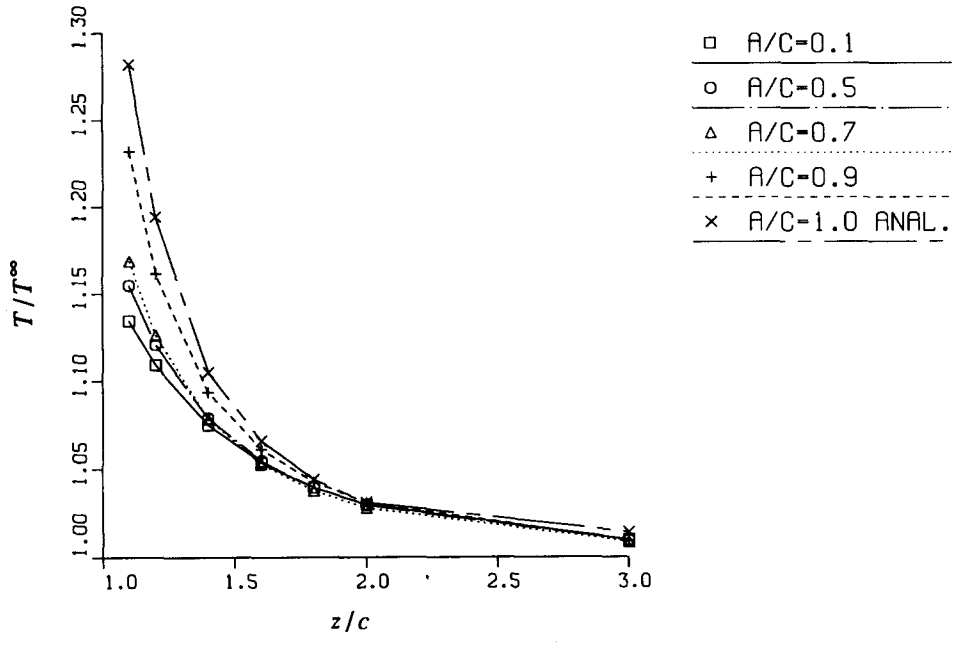

Figure 13. Rotational period of inertialess particles in a shear flow near a wall.

4. CONCLUSIONS

The forces and torques acting on spheroidal particles near the wall can be rationalized by comparing them with the interactions of:

(i) spheres near the wall,

(ii) spheroids far from the wall.

Comparison with the data for spheres yields that the effect of the wall on the forces and torques and the corresponding component of the friction tensor decrease when particle shape deviates from spherical. The wall effect on all interactions of needle-like oblong particles is small. For oblique angles of attack the wall effect on these particles is localized on their (small) portions, which are closest to the wall surface. The flow around the particle part which protrudes far from the wall is actually unaffected by its presence.

The effect of the wall leads to appearance of several viscous interactions which do not exist for spherical particles (i.e. the coupling components C_{yx}, C_{yz} of the friction tensor). On the other hand, for very small aspect ratios (oblong particles) these interactions disappear, in accordance with the above conclusion. These interactions reach their maxima for intermediate aspect ratios, of order 0.7–0.8.

The tensor coefficients K_{zz}, K_{xx}, K_{xz} and Ω_{yy}, as well as the lift, F_z and the drag, F_x forces near the wall, depend on θ in the same manner as their corresponding unbounded fluid counterparts. This allowed development of relatively simple correlations for the above quantities in wide ranges of the dimensionless distance from the wall, orientation angle and aspect ratio (see appendix B). These formulae may be used in various applications for calculating trajectories of nonspherical particles experiencing hydrodynamic interactions with a solid wall.

The forces calculated for spheroidal particles in a shear flow were used to calculate their translational and rotational velocities in circumstances where the particle characteristic relaxation time is small (inertia-free particles). It is known that the wall tends to retard a spherical particle translating parallel to the wall surface. It was found that for nonspherical particles this retgardation velocity is almost independent of orientation. The retardation velocity diminishes with decreasing aspect ratio and is negligible for spheroids with $a/c = 0.1$.

In contrast with spheres, spheroidal particles placed in a shear flow near a wall acquire a nonzero lift velocity, w, which is perpendicular to the streamlines. It vanishes far from the wall and also

in the two extremes of spherical and needle-like particles. The maximum value of w prevails at intermediate aspect ratios $a/c \sim 0.45$. Since w vanishes for oblong particles, they will rotate in a shear flow near a wall without drifting between the streamlines.

The effect of the wall is to diminish the particle angular velocity (retard its rotational motion), with the strongest effect prevailing for spherical particles. The influence of the increasing particle nonsphericity (decreasing a/c) is to diminish this rotational retardation. Therefore, a nonspherical particle immersed in a shear flow near a wall rotates more slowly than it will in a free shear flow. On the other hand, of all spheroidal particles with the same longer axis rotating near the wall, the particle with $a/c \sim 0.9$ exhibits the highest absolute rotation rate.

Acknowledgements—This work was in part supported by the Israel Ministry of Sciences and Humanities and by the fund for the promotion of research at the Technion.

REFERENCES

Bernstein, O. and Shapiro, M. (1994) Direct determination of the orientation distribution function of cylindrical particles immersed in laminar and turbulent shear flows. *J. Aerosol Science* **25,** 113–136.

Blake, J. R. (1971) A note on the image system for a Stokeslet in a no-slip boundary. *Proc. Camb. Phil. Soc.* **70,** 303–310.

Brenner, H. (1961) Slow motion of a sphere through a viscous fluid towards a plane surface. *Chem. Eng. Sci.* **16,** 242–251.

Brenner, H. and O'Neill M. E. (1972) On the Stokes resistance of multiparticle systems in a linear shear field. *Chem. Eng. Sci.* **27,** 1421–1439.

Brown R. C. (1993) *Air Filtration. An Integrated Approach to the Theory and Applications of Fibrous Filters*. Pergamon, Oxford.

Dabros, T. (1985) A singularity method for calculating hydrodynamic forces and particle velocities in low Reynolds number flows. *J. Fluid Mech.* **156,** 1–21.

Ganatos, P., Pfeffer, R. and Weinbaum, S. (1980) A strong interaction theory for the creeping motion of a sphere between parallel boundaries. Part I. Perpendicular motion. *J. Fluid Mech.* **99,** 739–753.

Gavze, E. (1990a) The accelerated motion of rigid bodies in nonsteady Stokes' flow. *Int. J. Multiphase Flow* **16,** 153–166.

Gavze, E. (1990b) A boundary integral equation solution of the Stokes' flow due to the motion of an arbitrary body near a plane wall with a hole. *Int. J. Multiphase Flow* **16,** 529–543.

Gerald, C. F. and Wheatley, P. O. (1989) *Applied Numerical Analysis*. Addison-Wesley, Reading, MA.

Goldman, A. J., Cox, R. J. and Brenner, H. (1967a) Slow viscous motion of a sphere parallel to a plane wall I. Motion through a quiescent fluid. *Chem. Eng. Sci.* **22,** 637–651.

Goldman, A. J., Cox, R. J. and Brenner, H. (1967b) Slow viscous motion of a sphere parallel to a plane wall II. Couette flow. *Chem. Eng. Sci.* **22,** 653–660.

Goldman, A. J. (1966) Ph.D. dissertation, New York University.

Happel, H. and Brenner, H. (1983) *Low Reynolds Number Hydrodynamics with Special Application to Particulate Media*. Noordhoff, Leyden.

Hinch, E. J. and Leal, L. G. (1979) Rotation of small nonaxisymmetric particles in a simple shear flow. *J. Fluid Mech.* **92,** 591–608.

Hsu, R. and Ganatos, P. (1989) The motion of a rigid body in viscous fluid bounded by a plane wall. *J. Fluid Mech.* **207,** 29–72.

Ingham, D. B. and Yan, B. (1994) Entrainment of particles on the outer wall of a cylindrical blunt sampler. *J. Aerosol Sci.* **25,** 327–340.

Jeffery, G. B. (1922) The motion of ellipsoidal particles immersed in a viscous fluid. *Proc. Roy. Soc. Lond.* **A102,** 161–179.

Jeffrey, D. J. and Onishi, Y. (1981) The slow motion of a cylinder next to a plane wall. *Q. J. Mech. Appl. Math.* **34,** 129–137.

Karrila, S. J. and Kim, S. (1989) Integral equations of the second kind for Stokes' flow: Direct

solution for physical variables and removal of inherent accuracy limitations. *Chem. Eng. Comm.* **82,** 123–161.

Keh, H. J. and Tseng, C. H. (1994) Slow motion of an arbitrary axisymmetric body along its axis of revolution and normal to a plane surface. *Int. J. Multiphase Flow* **20,** 185–210.

Kim, S. and Karrila, S. J. (1991) *Microhydrodynamics: Principles and Selected Applications*. Butterworth-Heinemann, Boston, MA.

Ladyzhenskaya, O. A. (1963) *The Mathematical Theory of Viscous Incompressible Flow*. Gordon and Breach, New York.

O'Neill, M. E. (1964) A slow motion of viscous liquid caused by a slowly moving solid sphere. *Mathematica* **11,** 67–74.

Shapiro, M. and Goldenberg, M. (1993) Deposition of glass fiber particles from turbulent air flow in a pipe. *J. Aerosol Sci.* **24,** 65–87.

Yu, C. P., Zhang, L., Oberdörster, G., Mast, R. W., Glass, L. R. and Utell, M. J. (1994) Deposition modelling of refractory ceramic fibers in the rat lung. *J. Aerosol Sci.* **25,** 407–418.

Yuan, F. and Wu, W. (1987) Stokes' flow of an arbitrary prolate axisymmetric body towards an infinite plane wall. *Appl. Math. Mech.* **8,** 17–30.

APPENDIX A

Forces and Velocities of Ellipsoidal Particles in an Unbounded Shear Flow

Here we summarize results for the hydrodynamic forces and torques acting on prolate spheroids in an unbounded shear flow, as well as velocities of inertialess particles.

First we will refer to a spheroid, described by the equation

$$\frac{x^2}{a^2}+\frac{y^2}{b^2}+\frac{z^2}{c^2}=1, \qquad \text{[A1]}$$

whose symmetry axis is parallel to the z-axis, which have $a=b$, $c/a>1$. Define the following parameters

$$\chi=\frac{a^2c}{\sqrt{c^2-a^2}}\ln\left[\frac{c+\sqrt{c^2-a^2}}{c-\sqrt{c^2-a^2}}\right],$$

$$\alpha=\frac{c^2}{c^2-a^2}-\frac{a^2c}{2(c^2-a^2)^{3/2}}\ln\left[\frac{c+\sqrt{c^2-a^2}}{c-\sqrt{c^2-a^2}}\right],$$

$$\gamma=\frac{-2a^2}{c^2-a^2}+\frac{a^2c}{(c^2-a^2)^{3/2}}\ln\left[\frac{c+\sqrt{c^2-a^2}}{c-\sqrt{c^2-a^2}}\right].$$

The diagonal elements of the translational resistance tensor **K** are (Happel and Brenner 1983):

$$K'_{xx}=K'_{yy}=\frac{16\pi\mu a^2c}{\chi+a^2\alpha}, \quad K'_{zz}=\frac{16\pi\mu a^2c}{\chi+c^2\gamma}, \qquad \text{[A2]}$$

and the off-diagonal elements of **K** are zero.

The diagonal elements of the rotation tensor are

$$\Omega_{xx}=\Omega_{yy}=\frac{16\pi\mu a^2c}{3}\frac{a^2+c^2}{a^2\alpha+c^2\gamma}, \quad \Omega_{zz}=\frac{16\pi\mu a^2c}{3\alpha}. \qquad \text{[A3]}$$

A stationary ellipsoid in a Stokes flow experiences the force (Happel and Brenner 1983):

$$\mathbf{F}=\mathbf{K}\cdot\left[\mathbf{u}_o+\frac{1}{3!}(\mathbf{D}^2\mathbf{u})_o+\frac{1}{5!}(\mathbf{D}^4\mathbf{u})_o+\cdots+\frac{1}{(2n+1)!}(\mathbf{D}^{2n}\mathbf{u})_o+\cdots\right], \qquad \text{[A4]}$$

where the subscript o refers to the center of the ellipsoid and D^2 is a differential operator

$$D^2 = a^2 \frac{\partial^2}{\partial x^2} + a^2 \frac{\partial^2}{\partial y^2} + c^2 \frac{\partial^2}{\partial z^2}. \qquad [A5]$$

The torque, acting on a stationary ellipsoid relative to its center o (Happel and Brenner 1983) is:

$$\mathbf{T}_o = \mathbf{Q} \cdot \left[(\diamondsuit \times \mathbf{u})_o + \frac{3!2}{5!} (D^2 \diamondsuit \times \mathbf{u})_o + \frac{3!3}{7!} (D^4 \diamondsuit \times \mathbf{u})_o + \cdots \right], \qquad [A6]$$

where $\mathbf{Q}$ is a diagonal tensor

$$Q_{xx} = Q_{yy} = \frac{\Omega_{xx}}{a^2 + c^2}, \quad Q_{zz} = \frac{\Omega_{zz}}{2a^2} \qquad [A7]$$

and $\diamondsuit$ is a vector differential operator

$$\diamondsuit = \mathbf{i}_x a^2 \frac{\partial}{\partial x} + \mathbf{i}_y a^2 \frac{\partial}{\partial y} + \mathbf{i}_z c^2 \frac{\partial}{\partial z}. \qquad [A8]$$

For a shear flow only the first terms in [A4] and [A6] differ from zero.

Consider now an ellipsoid whose axis of symmetry lies in the (x, z) plane and forms an angle θ with the positive direction of the z-axis (see figure 1). Denoting the body-fixed coordinates by $'$, and defining the orientation transition matrix M

$$M = \begin{bmatrix} \cos\theta & 1 & -\sin\theta \\ 0 & 1 & 0 \\ \sin\theta & 0 & \cos\theta \end{bmatrix}, \qquad [A9]$$

one has the following transformations between the body-fixed and laboratory frame coordinates

$$\mathbf{u}' = M\mathbf{u}, \quad \mathbf{K} = M^{-1}\mathbf{K}'M, \quad \mathbf{\Omega} = M^{-1}\mathbf{\Omega}'M. \qquad [A10]$$

Specifically, we will have for $\mathbf{K}$

$$\mathbf{K} = \begin{bmatrix} K'_{xx}\cos^2\theta + K'_{zz}\sin^2\theta & 0 & \frac{1}{2}(K'_{zz} - K'_{xx})\sin 2\theta \\ 0 & K'_{yy} & 0 \\ \frac{1}{2}(K'_{zz} - K'_{xx})\sin 2\theta & 0 & K'_{xx}\sin^2\theta + K'_{zz}\cos^2\theta \end{bmatrix}, \qquad [A11]$$

with K'_{xx}, K'_{zz} given by [A2]. Therefore, the force acting on the spheroid in a shear flow

$$\mathbf{u} = \begin{pmatrix} sz \\ 0 \\ 0 \end{pmatrix} \qquad [A12]$$

is obtained from [A4], [A11], [A12] in the form:

$$\mathbf{F} = \begin{bmatrix} K'_{xx}\cos^2\theta + K'_{zz}\sin^2\theta \\ 0 \\ \frac{1}{2}(K'_{zz} - K'_{xx})\sin 2\theta \end{bmatrix} sz. \qquad [A13]$$

The transformation of $\mathbf{\Omega}$ is the same as for $\mathbf{K}$ (see [A11]). In the present case the only term of interest is Ω_{yy} which remains unchanged. The torque in the space frame is:

$$\mathbf{T}_o = M^{-1}\mathbf{Q}'\cdot(\diamondsuit' \times M\mathbf{u}) = M^{-1}(\mathbf{Q}' \times \diamondsuit')\cdot M\mathbf{u}. \tag{A14}$$

One can further calculate

$$\mathbf{Q}' \times \diamondsuit' = \begin{bmatrix} 0 & -Q'_{xx}c^2\frac{\partial}{\partial z'} & -Q'_{xx}b^2\frac{\partial}{\partial y'} \\ -Q'_{yy}c^2\frac{\partial}{\partial z'} & 0 & -Q'_{yy}a^2\frac{\partial}{\partial x'} \\ -Q'_{zz}b^2\frac{\partial}{\partial y'} & -Q'_{zz}a^2\frac{\partial}{\partial x'} & 0 \end{bmatrix}. \tag{A15}$$

The shear flow [A12] is transformed to

$$M\mathbf{u} = \begin{pmatrix} sz\cos\theta \\ 0 \\ sz\sin\theta \end{pmatrix}. \tag{A16}$$

$$\frac{\partial z}{\partial x'} = M_{13} = -\sin\theta, \quad \frac{\partial z}{\partial y'} = M_{23} = 0, \quad \frac{\partial z}{\partial z'} = M_{33} = \cos\theta. \tag{A17}$$

After substituting the above formulae in [A14] we obtain the following expressions for the torque in the space frame

$$\mathbf{T}_o = s\begin{pmatrix} 0 \\ Q'_{yy}(c^2\cos^2\theta + a^2\sin^2\theta) \\ 0 \end{pmatrix}. \tag{A18}$$

The velocities of inertialess particles are determined from [21]. For ellipsoids in an unbounded fluid the coupling tensor is zero. Substitution of [A11], [A13] and [A18] in [21] yields

$$\begin{bmatrix} u \\ w \\ \omega \end{bmatrix} = s\begin{pmatrix} z \\ 0 \\ \dfrac{c^2\cos^2\theta + a^2\sin^2\theta}{c^2 + a^2} \end{pmatrix}. \tag{A19}$$

One can see that at $\theta = \pm\pi/4$ $\omega = 1/2$ for all values of the aspect ratio a/c.

Upon substitution $\omega = \mathrm{d}\theta/\mathrm{d}t$, one obtains from [A19] the following equation for θ:

$$\frac{\mathrm{d}(2\theta)}{\mathrm{d}t} = s\left[\left(1 + \frac{1-\gamma^2}{1+\gamma^2}\right)\cos(2\theta)\right], \tag{A20}$$

which subject to the initial condition $\theta(0) = 0$ possesses the solution:

$$\theta(t) = \arctan\left[\frac{1}{\gamma}\tan\left(s\frac{\gamma t}{1+\gamma^2}\right)\right]. \tag{A21}$$

One can see that the above is a periodic function with period

$$T^{\infty} = \frac{2\pi}{s}\left(\gamma + \frac{1}{\gamma}\right), \tag{A22}$$

which clearly reproduces the result of Jeffrey (1922) (see also Hinch and Leal 1979).

APPENDIX B

Correlation Formulae for Forces and Resistance Tensor Components

On the basis of the analyses of results, we propose simple analytical approximations for the various components, obtained by the regression analyses. For brevity we denote $\gamma = a/c$ and $\bar{z} = z/c$. The accuracy of the proposed formulae is evaluated by comparing approximate analytical, ($\tilde{f}$) and calculated numerical value (f) of the corresponding components. Explicitly, two types of errors are calculated: The integral error (based on the L_2 norm)

$$E_2(f) = \left[\int_a^b [f(x) - \tilde{f}(x)]^2 \, dx \right]^{1/2} \left[\int_a^b [f(x)]^2 \, dx \right]^{-1/2} \quad [B1]$$

and the maximal error E_∞:

$$E_\infty(f) = \max_{a \le x \le b} \left| \frac{f(x) - \tilde{f}(x)}{f(x)} \right|. \quad [B2]$$

Perpendicular (lift) force component F_z

Analysis of the numerical data shows that the ratio F_z/F_z^∞ is almost independent of θ. This suggests an approximation

$$\frac{F_z}{F_z^\infty} = 1 + \frac{0.43 + 1.53\gamma}{\bar{z}} + \frac{0.66\gamma}{\bar{z}^2}, \quad [B3]$$

which is valid for $0.1 < a/c < 0.9$ with errors $E_2 = 0.009$ and $E_\infty = 0.09$.

Parallel (drag) force F_x

We will approximate F_x in the form:

$$\frac{F_x}{\mu c s z} = Q(\bar{z}, \gamma)\cos 2\theta + R(\bar{z}, \gamma). \quad [B4]$$

In view of [28] Q vanish as $\gamma \to 1$, so that $R(\bar{z}, 1)$ represents the force acting on a sphere. The following approximations are sought for these two functions:

$$Q(\bar{z}, \gamma) = (a_1 + b_1\gamma + c_1\gamma^2) + \frac{1}{\bar{z}}(a_2 + b_2\gamma + c_2\gamma^2), \quad [B5a]$$

$$R(\bar{z}, \gamma) = (d_1 + e_1\gamma + f_1\gamma^2) + \frac{1}{\bar{z}}(d_2 + e_2\gamma + f_2\gamma^2). \quad [B5b]$$

Table B1 shows least square approximations for the coefficients appearing in [B5a, b].

Table B1. Computed values of the coefficients in [B5a, b] for $1.1 < \bar{z} < 10$

	a_i	b_i	c_i	d_i	e_i	f_i	E_2	E_∞
$i = 1$	1.158	− 0.237	− 0.971	4.627	15.91	− 2.193	0.005	0.03
$i = 2$	0.235	2.702	− 2.91	0.643	5.960	6.295	0.005	0.03

One can see that the least squares method indeed yields $Q(\bar{z}, 1)$ indeed close to zero. In table B2 we compare the values of $R(\bar{z}, 1)$ with our computed results for a sphere.

Table B2. Comparison between the approximated and computed values of $F_x/\mu csz$ for a sphere

$\bar{z}$	1.1	1.2	1.5	2	3	5	10
$F_x/\mu cSz$	30.54	29.49	27.19	24.93	22.72	21.03	19.84
$R(\bar{z}, 1)$	30.07	29.09	26.94	24.79	22.64	20.92	19.63

Torque T_y

The approximation is sought in the form

$$\frac{T_y - T_y^{\infty}}{\mu sc^3} \sim \sum_{i=1}^{2} \frac{1}{\bar{z}^i} \{[a_i\gamma + b_i\gamma^2 + c_i\gamma^2 \sin(\pi\gamma)]\cos 2\theta + [d_i + e_i\gamma + f_i\gamma^2]\}. \quad [B6]$$

The regression and the E_2 are presented in table B3 for $1.1 \leqslant \bar{z} \leqslant 10$. The E_∞ error is not given since it becomes infinite in cases where $T_y - T_y^{\infty}$ vanishes at $\theta = 0.3\pi$

Table B3. The regression coefficient and the error for $(T_y - T_y^{\infty})/\mu sc^3$

	a_i	b_i	c_i	d_i	e_i	f_i	E_2
$i = 1$	−3.11	3.04	−1.34	−0.056	−0.261	0.444	0.033
$i = 2$	0.488	−0.432	0.784	−0.069	0.272	−1.016	

Friction coefficient K_{zz}

An approximation is sought in the form

$$\frac{K_{zz}}{K_{zz}^{\infty}} \sim \frac{1}{\bar{z}^2}[a + b\gamma + c\gamma^2]\cos 2\theta + d_1 + \frac{d_2}{\bar{z}} + \frac{d_3}{\bar{z}^2} + \frac{1}{\bar{z}^2}[e\gamma + f\gamma^2]. \quad [B7]$$

Table B4 shows the regression coefficients and the error for the three domains: $1.1 \leqslant \gamma \leqslant 0.95$, $0 \leqslant \theta \leqslant 0.5\pi$ and $1.1 \leqslant \bar{z} \leqslant 10$, $1.2 \leqslant \bar{z} \leqslant 10$, $1.3 \leqslant \bar{z} \leqslant 10$.

Table B4. The regression coefficients and errors for K_{zz}/K_{zz}^{∞}

	a	b	c	d_1	d_2	d_3	e	f	E_2	E_∞
$1.1 \leqslant \bar{z} \leqslant 10$	−0.195	0.611	0.030	1.120	−0.403	1.068	0.437	4.523	0.07	0.40
$1.2 \leqslant \bar{z} \leqslant 10$	−0.178	0.397	−0.034	1.069	0.035	0.389	1.389	2.999	0.03	0.24
$1.3 \leqslant \bar{z} \leqslant 10$	−0.171	0.242	0.034	1.046	0.245	0.030	1.867	2.273	0.02	0.16

Friction coefficient K_{xx}

We look for an approximation in the form

$$\frac{K_{xx}}{K_{xx}^{\infty}} \sim [a(\bar{z}) + b(\bar{z})\gamma + c(\bar{z})\gamma^2]\cos 2\theta + d(\bar{z}) + e(\bar{z})\gamma + f(\bar{z})\gamma^2. \quad [B8]$$

For the domain $1.1 \leqslant \gamma \leqslant 0.95$, $1.1 \leqslant \bar{z} \leqslant 10$, $0 \leqslant \theta \leqslant 0.5\pi$ the following approximation is found by the least squares fit:

$$\frac{K_{xx}}{K_x^{\infty}} = \frac{0.061 + 0.311\gamma - 0.338\gamma^2}{\bar{z}^2}\cos 2\theta + 1.012 + \frac{0.255}{\bar{z}} + \frac{-0.178 + 0.858\gamma + 0.303\gamma^2}{\bar{z}^2}. \quad [B9]$$

The accuracy of this approximation is characterized by the integral error $E_2 = 0.011$ and the maximum error $E_\infty = 0.061$. Of 742 points used only at 16 the error exceeded 0.05. These points were all located at $\bar{z} = 1.1$, $0 \leqslant \theta \leqslant \pi/4$ and $0.3 \leqslant \gamma \leqslant 0.95$.

Friction coefficient K_{xz}

The ratio K_{xz}/K_{xz}^{∞} is approximated by

$$\frac{K_{xz}}{K_{xz}^{\infty}} \sim \frac{1}{\bar{z}^2}[a + b\gamma + c\gamma^2]\cos(2\theta) + d_1 + \frac{d_2}{\bar{z}} + \frac{1}{\bar{z}^2}[d_3 + e\gamma + f\gamma^2]. \qquad [B10]$$

The regression coefficients and the errors for the domains $0.1 \leqslant \gamma \leqslant 0.95$, $0.05\pi \leqslant \theta \leqslant 0.45\pi$, $1.1 \leqslant \bar{z} \leqslant 10$ and $1.2 \leqslant \bar{z} \leqslant 10$ are given in table B5.

Formula [B10] is not valid for orientations $\theta = 0$ and $\theta = \pi/2$ since at these angles $K_{xz}^{\infty} = 0$. For both cases, the largest errors are restricted to a few points only.

Table B5. The regression coefficients and errors for K_{xz}/K_{xz}^{∞}

	a	b	c	d_1	d_2	d_3	e	f	E_2	E_∞
$1.1 \leqslant \bar{z} \leqslant 10$	−0.086	0.725	−0.307	1.083	0.299	0.124	2.718	3.469	0.04	0.42
$1.2 \leqslant \bar{z} \leqslant 10$	−0.129	0.852	−0.659	1.056	0.535	−0.234	3.045	2.911	0.02	0.14

Friction coefficient Ω_{yy}

This can be approximated in the form

$$\frac{\Omega_{yy}}{\Omega_{yy}^{\infty}} \sim d_1 + \frac{d_2}{\bar{z}} + \frac{d_3 + e\gamma + f\gamma^2}{\bar{z}^2}. \qquad [B11]$$

The values of the regression coefficients and the errors in the domain $0.1 \leqslant \gamma \leqslant 0.95$ $0 \leqslant \theta \leqslant \pi/2$ $1.1 \leqslant \bar{z} \leqslant 10$ are given in table B6.

Table B6. Regression coefficients and errors for $\Omega_{yy}/\Omega_{yy}^{\infty}$

d_1	d_2	d_3	e	f	E_2	E_∞
1.012	−0.137	0.264	0.116	0.054	0.007	0.11

Coupling coefficient C_{yx}

We seek an approximation for C_{yx} in the form

$$\frac{C_{yx}}{\mu c^2} \sim \frac{1}{\bar{z}^n}[a\gamma + b\gamma^2 + c\gamma^4]\cos(2\theta) + \sum_{i=0}^{n} \frac{d_{i+1}}{\bar{z}^i} + \frac{1}{\bar{z}^n}[e\gamma + f\gamma^2]. \qquad [B12]$$

The approximation may be used in different regions, namely in $1.2 \leqslant \bar{z} \leqslant 1.6$ (with $n = 3$) and in $1.6 < \bar{z} \leqslant 10$ (with $n = 2$).

The values of the regression coefficients and the error E_2 are given in table B7. The error E_∞ may not be given since it becomes infinitely large when $C_{yx} = 0$.

Table B7. Regression coefficients and errors for C_{yx}

	a	b	c	d_1	d_2	d_3	d_4	e	f	E_2
$1.2 \leqslant \bar{z} \leqslant 1.6$	−3.91	−1.43	5.03	2.90	−13.49	21.27	−11.43	−1.08	−0.13	0.07
$1.6 < \bar{z} \leqslant 10$	−2.65	−0.118	2.69	−0.011	0.142	−0.366	—	−0.424	0.209	0.08

Coupling coefficient C_{yz}

This coefficient was approximated by:

$$\frac{C_{yz}}{\mu c^2} \sim \{[a_1\gamma^{1/2} + (b_1 + c_1\gamma^2)\sin(\pi\gamma)]\sin(2\theta) + d_1\gamma^2 \sin(\pi\gamma)\sin(4\theta)\}\frac{1}{\bar{z}^2}$$

$$+ \{[a_2\gamma^{1/2} + (b_2 + c_2\gamma^2)\sin(\pi\gamma)]\sin(2\theta) + d_2\gamma^2 \sin(\pi\gamma)\sin(4\theta)\}\frac{1}{\bar{z}^3}. \qquad [B13]$$

The regression coefficients and the error E_2 are given in table B8.

It may be clearly seen that the second harmonic $\sin(4\theta)$ has a small weight in the approximation for $\bar{z} > 1.6$.

Table B8. Regression coefficients and the error for C_{zv}

Range	a_1	b_1	c_1	d_1	a_2	b_2	c_2	d_2	E_2
$1.2 \leqslant \bar{z} \leqslant 1.6$	−4.61	4.62	−10.20	−4.55	7.97	−5.47	23.47	7.32	0.05
$1.6 \leqslant \bar{z} \leqslant 10$	0.016	1.16	0.767	−0.165	0.785	−0.105	5.834	0.483	0.03